AGU ADVANCING EARTH AND SPACE SCIENCE

Water Resources Research

RESEARCH ARTICLE
10.1029/2022WR032067

Vegetation Index-Based Partitioning of Evapotranspiration Is Deficient in Grazed Systems

Pushpendra Raghav[1], Pradeep Wagle[2], Mukesh Kumar[1], Tirtha Banerjee[3], and James P. S. Neel[2]

[1]Department of Civil, Construction, and Environmental Engineering, University of Alabama, Tuscaloosa, AL, USA, [2]USDA, Agricultural Research Service, Grazinglands Research Laboratory, El Reno, OK, USA, [3]Department of Civil and Environmental Engineering, University of California, Irvine, CA, USA

Key Points:

- Three Evapotranspiration (ET) partitioning methods were used to partition ET in differently managed wheat systems
- Grazing altered the relation between T:ET and enhanced vegetation index
- ET partitioning errors were higher in disturbed (i.e., grazed) systems

Supporting Information:

Supporting Information may be found in the online version of this article.

Correspondence to:

M. Kumar,
mkumar4@eng.ua.edu

Citation:

Raghav, P., Wagle, P., Kumar, M., Banerjee, T., & Neel, J. P. S. (2022). Vegetation index-based partitioning of evapotranspiration is deficient in grazed systems. *Water Resources Research*, *58*, e2022WR032067. https://doi.org/10.1029/2022WR032067

Received 25 JAN 2022
Accepted 9 AUG 2022

Author Contributions:

Conceptualization: Pushpendra Raghav, Mukesh Kumar
Data curation: Pushpendra Raghav, Pradeep Wagle
Formal analysis: Pushpendra Raghav, Mukesh Kumar
Funding acquisition: Mukesh Kumar
Investigation: Pushpendra Raghav, Mukesh Kumar
Methodology: Pushpendra Raghav, Mukesh Kumar
Project Administration: Mukesh Kumar
Resources: Pradeep Wagle, James P. S. Neel
Software: Pushpendra Raghav
Supervision: Mukesh Kumar
Validation: Pushpendra Raghav
Visualization: Pushpendra Raghav
Writing – original draft: Pushpendra Raghav
Writing – review & editing: Pushpendra Raghav, Pradeep Wagle, Mukesh Kumar, Tirtha Banerjee

Abstract Partitioning evapotranspiration (ET) into its primary components, that is, evaporation (*E*) and plant transpiration (*T*), is needed in a range of hydrometeorological applications. Using vegetation index (VI) to obtain spatially resolved T:ET ratio over large areas has emerged as a promising approach in this regard. Here, we assess the effectiveness of this approach in differently managed wheat systems. Results show a weak relation between T:ET and VI in disturbed (i.e., grazed) systems. Furthermore, flux partition based on a canonical T:ET versus VI relation or the relation derived in a neighboring undisturbed wheat system introduce large errors in disturbed systems, thus underscoring the limits on the transferability of the VI-based ET partitioning approach. The effectiveness of the VI-based approach is found to be related to the strength of correlation between VI and vapor pressure deficit and/or radiation. This correlation metric can help identify settings where the approach is likely to be effective.

Plain Language Summary Evapotranspiration (ET) plays a significant role in water and climate cycles by affecting the energy and water balance over the land surface which in turn mediates the land-atmosphere interactions. ET is composed of two primary components that is, direct evaporation (*E*) and plant transpiration (*T*). Partitioning total ET into its individual components (*E* and T) is of significant importance for better assessment of both regional and global water budgets. One of the primary approaches to partition ET over large areas is by using vegetation indices (VI), which indirectly capture plants' biophysical state. This approach has been used to partition ET in different landscapes, but its efficacy has not been tested in disturbed ecosystems, which cover a large fraction of Earth's vegetated area. Here, we assess the effectiveness of this VI-based ET partitioning approach in disturbed (i.e., grazed) ecosystems. We find that the VI-based ET partitioning introduces large errors in disturbed systems. Further investigation identifies conditions that can be used to filter-out regions where the VI-based partition is likely to be more (or less) effective.

1. Introduction

Around 60% of the precipitated water is returned to the atmosphere by evapotranspiration (ET) (Oki & Kanae, 2006). Unsurprisingly, ET plays a major role in influencing the water and climate cycles components at both local and global scales (Bonetti et al., 2015; Condon & Maxwell, 2019; Jung et al., 2010; Oishi et al., 2010; R. Wang et al., 2013; Zhang et al., 2016). To assess these influences, it is crucial to partition ET into its components, viz. evaporation (*E*) from bare soil and wet plant surfaces, and plant transpiration (*T*). This is especially needed as relative contributions of *E* and *T* vary in space and time, in part due to the varied controls on *E* and *T* (Ritchie & Burnett, 1971; Unkovich et al., 2018). For instance, in addition to the meteorological, soil, and plant morphometric properties that influence *E*, *T* is also majorly influenced by plant physiology (Y. Liu et al., 2017, 2020; X. Sun et al., 2019; Wang & Liu, 2007). Partitioning of ET can facilitate understanding of plants' water use strategies and their responses to environmental forcings, help assess the role of changes in land cover on ET, and improve predictions of hydrological responses as moisture used for *E* and *T* are usually derived from different soil stores (Alkama & Cescatti, 2016; X. Chen et al., 2015; Perez-Priego et al., 2018; Raghav & Kumar, 2021; Zeng et al., 2017).

Over the past years, several methods have been developed for ET partitioning to improve our understanding of the dynamics of *T* over ET (T:ET hereafter). Broadly, these methods can be categorized as direct and indirect. Direct methods use in situ observations of the water fluxes (i.e., *E*, *T*, and/or ET), and include eddy covariance (EC)

data based partitioning, sap flux and/or micrometeorological techniques (Cammalleri et al., 2013), microlysimeters and/or chambers (Yaseef et al., 2010), and techniques based on stable isotopes in the water fluxes (Ferretti et al., 2003; Williams et al., 2004; Xiao et al., 2018). Details on these various methods of partitioning and their challenges are well documented elsewhere (Kool et al., 2014; Stoy et al., 2019). Majority of the methods listed above provide T:ET estimates at the gauging sites (e.g., Black et al., 1969; Li et al., 2019; Nelson et al., 2020; Paul-Limoges et al., 2020; Perez-Priego et al., 2018; Scanlon & Sahu, 2008; Scott & Biederman, 2017; Zhou et al., 2016) or over its flow contribution area (e.g., Good et al., 2015; Jasechko et al., 2013). To obtain spatially explicit estimates of T:ET, numerous alternative indirect methods have been developed. For example, Long and Singh (2012) and Zhang et al. (2019) used a remote sensing approach to partition ET. Land surface modeling (e.g., Dirmeyer et al., 2006; Fatichi & Pappas, 2017; Haddeland et al., 2011; Lian et al., 2018; Paschalis et al., 2018) and hybrid approaches (e.g., Martens et al., 2017; Miralles et al., 2011) have also been used to obtain T:ET estimates over large areas. Recently, parsimonious models that only use widely available vegetation indices to obtain T:ET at multiple temporal scales (e.g., weekly, monthly, seasonal) has received significant attention (e.g., Berkelhammer et al., 2016; Fatichi & Pappas, 2017; S. Kang et al., 2003; L. Wang et al., 2014; Wei et al., 2015, 2017). These models are able to explain a significant fraction of variability in T:ET using vegetation indices such as leaf area index (LAI) and enhanced vegetation index (EVI). For example, based on a meta-analysis, Wei et al. (2017) reported that T:ET can be well represented as a function of LAI ($R^2 = 0.87$) in cropland settings. Zhou et al. (2016) showed that T:ET is strongly related to EVI ($R^2 = 0.85$) at eight-day scale based on the concept of underlying water use efficiency (uWUE). S. Kang et al. (2003) also reported a close relation between T:ET and LAI ($R^2 = 0.97$) in a winter wheat system based on lysimeter data. L. Wang et al. (2014) concluded that LAI and growth stage function can be used to obtain global T:ET estimates.

Notably, the efficacy of vegetation index based approach has not been tested in disturbed ecosystems or ecosystems that experience impulse alterations in canopy cover, such as due to grazing management, thinning, hurricanes, and wildfires. We furnish this gap by evaluating the relation between T:ET and vegetation index in both undisturbed and disturbed wheat systems. Here, the disturbance is introduced due to grazing management. In addition, we assess the conditions that facilitate a stronger correlation between T:ET and vegetation index. The paper is organized as follows: Section 2 provides a detailed description on the materials and methods used in this study. Results on the flux partitioning are presented in Section 3.1. Section 3.2 presents the results on the relationships between T:ET and EVI. The errors statistics in the prediction of T:ET using EVI at different time scales are presented in Section 3.3. Section 4.4 assesses the controls on T:ET versus vegetation index relation.

2. Materials and Methods

2.1. Study Sites

Two years of data from three neighboring, but differently managed, winter wheat cropping fields (Sites 1–3 hereafter) were used (Figure 1 and Figure S1 in Supporting Information S1). Each field (cropped area ranging from ∼13 to 22 ha) had identical soil type, experienced similar climatology, and the wheat seeds were sown at about 19 cm row spacing in each field. These fields are part of the United States Department of Agriculture, Agricultural Research Service, Grazinglands Research Laboratory's flux network (GRL-FLUXNET), which is a dense network of 16 Eddy Covariance (EC) towers in central Oklahoma (El Reno), USA. During the 2016–2017 growing season (October 2016–May 2017), grain-only and graze-grain wheat were grown at sites 1 and 3, respectively. Grain-only wheat has a single purpose to produce wheat grains, while graze-grain wheat has a dual purpose as it serves as a pasture for grazing cattle from November to February and is used for producing wheat grains thereafter. As data of differently managed configurations are only available for wheat, we restrict this study to wheat crops. Hence, 2016–2017 data from site 2, where Canola was grown, was not considered. In the 2017–2018 growing season, site 1 had graze-grain wheat, site 2 had grain-only wheat, and site 3 had graze-out wheat. Graze-out is also a single purpose crop that is grown for the entire season to solely serve as a pasture for the grazing cattle. The 2017–2018 growing season data from all three sites were used for analyses.

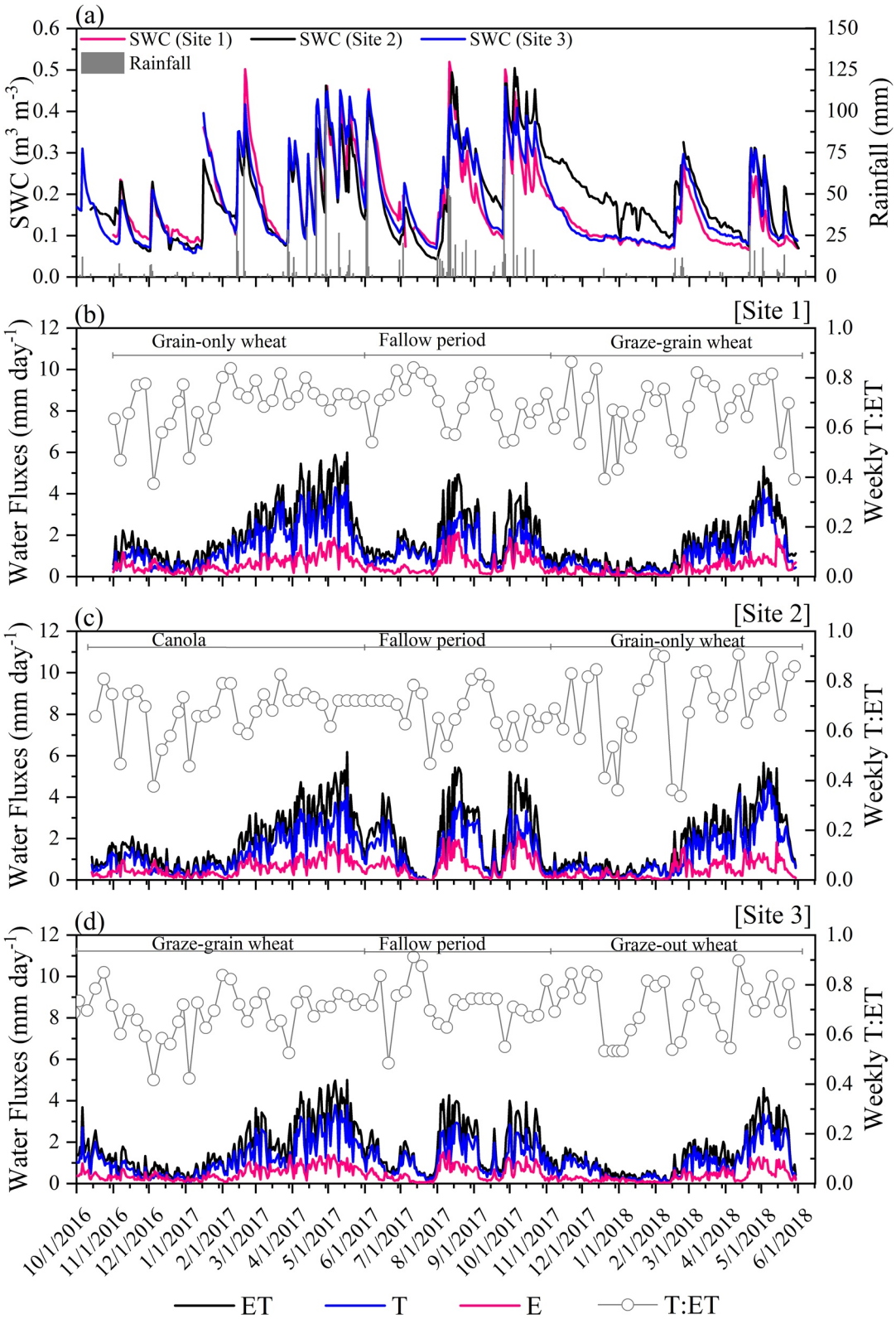

Figure 1. (a) Daily variations of rainfall and soil water content at each site, (b–d) daily variations of total evapotranspiration (ET), transpiration (*T*), and direct evaporation (*E*) based on flux variance similarity method at three different sites. Open circles plotted on the secondary *Y*-axis show the ratio of weekly *T* and ET. Notably, all three sites underwent crop rotation. Fallow period and canola were not considered for analyses in this study.

2.2. Data

2.2.1. Eddy Covariance and Ancillary Hydro-Meteorological Data

Water vapor and carbon dioxide fluxes were measured in all three wheat fields for the 2016–2017 and 2017–2018 growing seasons using eddy covariance (EC) systems. The data were recorded at 10 Hz frequency (i.e., 10 measurements per second) and then processed in the EddyPro software to get good quality estimates of latent heat fluxes at 30 min intervals. All the EC towers were located in the middle of respective fields. Measurement height of the EC system installed on the tower was about 2.5 m for all the sites. This resulted in fetch length to be around 100 m for more than 80% of the time during the growing period. More details on the EC data collection and processing can be found in Wagle et al. (2018, 2019).

Ancillary hydro-meteorological variables such as net radiation, soil water content (~5 cm depth), air temperature, soil heat flux, soil temperature, relative humidity, incoming photosynthetic photon flux density, and infrared surface temperature were also measured at the sites. We obtained rainfall data from the Oklahoma El Reno Mesonet station (located within 1–1.5 km from the study sites).

2.2.2. Remote-Sensing Data

The EVI for the three differently managed wheat systems, that is, grain-only, graze-grain, and graze-out, were derived (Figure S2 in Supporting Information S1) at 30 m spatial resolution using the Landsat surface reflectance images from both Landsat 7 ETM+ and Landsat 8 obtained from the U.S. Geological Survey (USGS) Earth Explorer. The EVI of individual pixels were spatially averaged for each field using ENVI software. The derived EVI data has a temporal resolution of 8 days (Figure S2 in Supporting Information S1). Data quality flag was used to select pixels within a field for any given date for further analyses. The EVI for each pixel was calculated following Jiang et al. (2008):

$$EVI = \frac{G \cdot (NIR - R)}{NIR + C1 \cdot R - C2 \cdot B + L} \tag{1}$$

where G (=2.5) is a gain factor. $C1$ (=6) and $C2$ (=7.5) are band-specific correction coefficients of aerosol resistance term. L (=1) is background brightness correction factor. NIR, R, and B are the near-infrared, red, and blue bands, respectively.

2.3. ET Partitioning

Total ET was partitioned into T and E based on three methods using the EC data sets: flux variance similarity (FVS) theory-based method (Scanlon & Sahu, 2008), the uWUE method (Zhou et al., 2016), and the transpiration estimation algorithm (TEA) method (Nelson et al., 2018). Consideration of multiple methods for this study was driven by the fact that estimates from no one method is generally considered perfect, and each of them are affected by inherent assumptions in them.

The FVS method can simultaneously partition ET and net ecosystem CO_2 exchange (NEE) into their primary components, that is, T and E for ET, and photosynthesis and respiration for NEE, based on the correlation between high-frequency EC measurements of carbon dioxide and water vapor fluxes along with measured or estimated leaf-scale water use efficiency (WUE) (Scanlon & Kustas, 2010, 2012; Scanlon & Sahu, 2008; Scanlon et al., 2019). Readers may refer to Text S1 in Supporting Information S1 and references therein for the mathematical formulation of FVS theory. The method has shown promising results in different land cover settings (Peddinti & Kambhammettu, 2019; Rana et al., 2018;Scanlon & Kustas, 2012; Sulman et al., 2016; Wagle et al., 2020; Wagle, Gowda, et al., 2021; L. Wang et al., 2010; W. Wang et al., 2016), including cropped systems such as rainfed alfalfa field (Wagle et al., 2020), Mediterranean cropping system (Rana et al., 2018), wheat (a $C3$ crop) (Scanlon & Sahu, 2008), corn (a $C4$ crop) (Scanlon & Kustas, 2010), and several others (Wagle, Skaggs, et al., 2021). One of the critical inputs to FVS method is the leaf-scale WUE. In the absence of direct measurements, leaf-scale WUE can be estimated as below:

$$WUE = \left(\frac{1}{DR}\right) \cdot \left(\frac{c_a - c_i}{q_a - q_i}\right) \tag{2}$$

where DR (=1.6) is the ratio of molecular diffusivities for water and carbon concentrations through the stomatal aperture (Massman, 1998). c_a (q_a) and c_i (q_i) are the ambient and intercellular concentrations of carbon (water), respectively. Here, c_a and q_a can be derived by extrapolating the logarithmic mean profile of EC measurements of carbon dioxide and water vapor fluxes with stability correction to zero displacement height (Brutsaert, 2013; Scanlon & Sahu, 2008). q_i is usually estimated assuming 100% relative humidity at leaf temperature (approximated as ±2°C of the air temperature). c_i can be modeled in different ways in Fluxpart (Wagle, Skaggs, et al., 2021). Based on the findings of Wagle, Skaggs, et al. (2021) for wheat, we choose a constant ratio method where c_i/c_a is assumed to be constant (K); with $K = 0.7$ for $C3$ plants (Sinclair et al., 1984) and $K = 0.44$ for $C4$ plants (Kim et al., 2006).

Water flux partitioning based on uWUE concept was proposed by Zhou et al. (2016). Herein, partitioning is performed based on uWUE, which is obtained using gross primary productivity (GPP) and vapor pressure deficit (VPD) based on Zhou et al. (2014):

$$uWUE = \frac{GPP \cdot \sqrt{VPD}}{ET} \tag{3}$$

T:ET is estimated as:

$$\frac{T}{ET} = \frac{uWUE_a}{uWUE_p} \tag{4}$$

where $uWUE_a$ is the apparent uWUE and $uWUE_p$ is the potential uWUE. $uWUE_a$ is estimated directly from Equation 3 if partitioning needs to be obtained at half-hour resolution. For estimates at coarser resolution (say a week or coarser), a linear regression between $GPP \cdot \sqrt{VPD}$ and ET is obtained using data derived through averaging of participating variables using a moving window approach. $uWUE_p$ represents the maximum carbon gain to water loss and is estimated using 95th quantile regression between $GPP \cdot \sqrt{VPD}$ and ET for a given year or season. The key assumption of uWUE-based method is that $uWUE_p$ is constant for a given year or season and calculation of $uWUE_p$ is based on periods when $T \approx$ ET or $E \approx 0$. uWUE-based method is very straightforward in nature and easy to use. This approach has been used to partition water fluxes in different biomes (Bai et al., 2019; Hu et al., 2018; Nelson et al., 2020; J.-Y. Sun et al., 2020; Xu et al., 2021; Zhou et al., 2016, 2018).

TEA method is a nonlinear machine learning method for water flux partitioning Nelson et al. (2018). TEA method predicts the T using a Random Forest (RF) regressor which is trained for ecosystem WUE (=GPP/ET) during dry periods of growing season that is, during periods when $E \approx 0$ or in other words the RF model is trained for GPP/T. The dry periods are selected by filtering out the wet periods from the time series based on rainfall and ET inputs. To ensure the good quality data for training the model, various quality control steps are performed, as detailed in Nelson et al. (2018). The trained model on the filtered data is then used to predict GPP/T for the full time series. TEA method has been shown to perform well across different ecosystems (Hu & Lei, 2021; Migliavacca et al., 2021; Nelson et al., 2018, 2020; Räsänen et al., 2020).

2.4. Modeling T:ET Ratio

Partitioning using all three methods was performed for two growing seasons (2016–2017 and 2017–2018) at three wheat sites. As site 2 had Canola planted in 2016–2017 (Figure 1), it was not considered in this study. The three partitioning methods have different data requirements to model T:ET. Partitioning from FVS method was performed using 10 Hz frequency EC data using Fluxpart version 0.2.10 (Skaggs et al., 2018). Partitioning from uWUE and TEA methods were performed using the 30 min interval flux data, which was obtained by processing high frequency EC data in EddyPro software (Wagle et al., 2018). The flux data was also processed with CO_2 flux partitioning (i.e., NEE to GPP and ecosystem respiration (R_{eco})) and gap filling using REddyProc package in R (Reichstein et al., 2005; Wutzler et al., 2018). Partition estimates were obtained at 30 min interval using all three methods. Fluxpart may fail to produce outputs for a certain intervals because of various physical constraints (Palatella et al., 2014; Scanlon et al., 2019; Wagle, Skaggs, et al., 2021). Other two methods may also produce erroneous values of T:ET for certain time periods. We only used reliable estimates of T:ET, and filtered out the bad quality estimates following the rubric detailed in Nelson et al. (2018) and Zhou et al. (2016). Also, the hours

with rainfall were removed from the analysis as partitioning estimates during it are expected to be unreliable. Overall, the application of aforementioned quality constraints resulted in 50%, 52%, and 81% of the data being suitable for further analyses for FVS, uWUE, and TEA methods, respectively. To obtain T:ET at weekly and monthly scales, weekly mean diurnal cycles were used. For example, to calculate the T:ET for a particular week, mean diurnal variations of T and ET at half-hour resolution were generated for the week, and then T:ET was determined by summing half-hourly binned mean T and mean ET. The resultant weekly average T:ET (a constant ratio for a week) was used to partition EC-measured daily ET values into daily E and T values. Seasonal T:ET was evaluated using seasonal T and ET estimates, which were obtained by summing individual daily estimates over a season.

2.5. Deriving T:ET Versus EVI Relation

Following the lead of previous studies (Lian et al., 2018; L. Wang et al., 2014; Wei et al., 2015, 2017), we derived a power-law relation ($T{:}ET = a\mathrm{EVI}^b$) between Landsat-derived EVI and weekly averaged T:ET from all the ET partitioning methods in all three wheat systems, that is, grain-only, graze-grain, and graze-out. As has also been done in the previous studies, binning of T:ET was carried out to reduce the effects of confounding variables (e.g., rainfall, available energy) on the emergent T:ET-EVI relation during the growing period. Best fit parameters a and b for each system were obtained by performing a nonlinear regression analysis using nonlinear least squares method in R (Bates & Watts, 1988; Elzhov et al., 2010).

3. Results and Discussion

3.1. Temporal Variations in T:ET

Weekly T:ET ratios were obtained for all three wheat sites for 2016–2018 using the three ET partitioning methods (see Figure 1, Figures S3 and S4 in Supporting Information S1). ET fluxes were larger during the 2016–2017 growing season than the 2017–2018 growing season at each site, in part because the former received much more rainfall. For example, total seasonal ET, that is, ET during November–May in 2016–2017 (2017–2018) for grain-only and graze-grain wheat were ∼460 mm (∼345 mm) and ∼367 mm (∼287 mm), respectively. Corresponding precipitation totals for the two seasons were 501 and 155 mm, respectively. Notably, the change in T:ET between the two seasons was modest with its magnitude being 0.71 (0.74) and 0.70 (0.7) in grain-only and graze-grain wheat in 2016–2017 (2017–2018) based on FVS method. Corresponding seasonal T:ET estimates using uWUE method were 0.58 (0.58) and 0.54 (0.55) in grain-only and graze-grain wheat. TEA method yielded seasonal T:ET of 0.80 (0.78) and 0.74 (0.76). Seasonal T:ET estimates obtained here, based on TEA and FVS methods, are consistent with other studies for winter wheat. For example, Ma and Song (2019) reported a seasonal T:ET of 0.75 based on the traces of stable isotopes. Yu et al. (2009), S. Kang et al. (2003), and C. Liu et al. (2002) reported a seasonal T:ET ranging between 0.67 and 0.75 based on microlysimeters. Notably, uWUE method shows a lower T:ET estimate with respect to TEA and FVS methods. The small difference in T:ET across the 2 years and wheat systems is consistent with the findings of past studies (Good et al., 2017; Nelson et al., 2020; Wagle, Gowda, et al., 2021), which attribute it to the reduction in canopy cover when faced with limiting resources, and to the compensating effect of E from wet canopies (intercepted rainfall) versus that from wet soil with changes in canopy cover. The T:ET was, however, found to be highly variable within the season (Figure 1). Weekly mean and coefficient of variation of T:ET, based on FVS method, were 0.63 (0.67) and 13.95% (20.33%), respectively, in 2016–2017 (2017–2018) at the grain-only site. The corresponding values for the graze-grain site were 0.62 (0.66) and 14.95% (14.45%). The intra-seasonal variations are attributable to a variety of hydroclimatic variables (e.g., rainfall, atmospheric water demand, available energy, and soil moisture). Overall, VPD, especially, had a strong control on T:ET variations with low T:ET values at low VPD and high values at high VPD. For example, average T:ET in grain-only wheat was 0.52 for low VPD values (VPD less than 25th percentile) and T:ET was 0.84 for high VPD values (VPD larger than 75th percentile). This is largely because seasonal VPD is correlated with increasing LAI. Larger biomass decreases the amount of radiative energy available for soil evaporation due to increased shading. At the same time, it also contributes to increase in transpiration. These result in higher T:E, and consequently T:ET, later in the growing season when the VPD is also higher. Another contributor to this variation is the occurrence of lower VPD periods post precipitation or dewfall during which soil is usually wet and T:ET is diminished (X. Sun et al., 2019). For example, T:ET was around 0.52 during rainy days as compared to 0.70 during non-rainy days in January 2017 (EVI is low during this period) for grain-only system. This is true

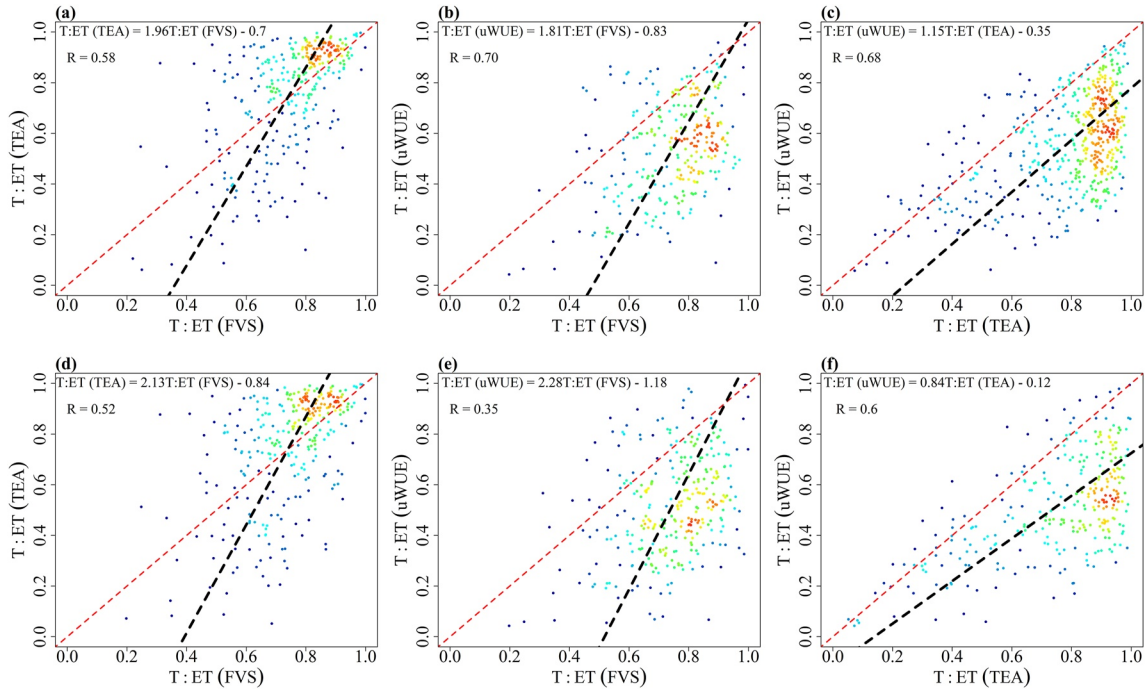

Figure 2. Intercomparison of the three evapotranspiration (ET) partitioning methods, viz. (a) T:ET (FVS) to T:ET (TEA), (b) T:ET (FVS) to T:ET (uWUE), and (c) T:ET (TEA) to T:ET (uWUE), at daily temporal resolution for the three sites. Panels (d–f) are similar to panels (a–c), respectively, but show the comparison only for the periods when ET partitioning estimates were available from all the three methods. *R* represents the Pearson correlation coefficient. The black dashed lines are the best fit linear lines estimated using orthogonal-least-squares regression (S. Chen et al., 1989). Notably, the data used for intercomparison only includes the period during which T:ET estimates are available for both the intercomparing methods. Colors of the data points represent the relative point density with warmer colors indicating higher density.

even for peak wheat growth period (Mid-March, 2017 to Mid-April, 2017; EVI is high during this period) when T:ET was about 0.64 during rainy days as compared to 0.82 during non-rainy days. During post precipitation time intervals, wetness of the top soil may enhance *E* more than *T*, as the root zone moisture available for transpiration may still be deficient. Furthermore, wetness on the leaves during these times may inhibit transpiration (Good et al., 2017; X. Sun et al., 2019). Notably, the increasing T:ET with VPD over a growing season, which is a result of covariation of multiple other variables as noted above, is in contrast to the expected T:ET variations with VPD for the scenario with negligible difference in LAI and other meteorological conditions.

Intercomparison of all the three methods for ET partitioning shows that there is agreement among the methods in regards to capturing the overall temporal pattern of T:ET, with a correlation of 0.58 between FVS and TEA, 0.70 between FVS and uWUE, and 0.68 between TEA and uWUE (Figure 2). Overall, uWUE method shows lower T:ET (with average T:ET = 0.54) as compared to T:ET estimates from FVS method (with average T:ET = 0.75), while the TEA method was in good agreement (with average T:ET = 0.76) with FVS method. These results for TEA and uWUE are in agreement with Nelson et al. (2020) where uWUE method also produced lower T:ET estimates as compared to the TEA method.

3.2. Relation Between T:ET and EVI

Following the method described in Section 2.5, the relation between T:ET and EVI was developed. We found that the EVI could explain most of the variability (44%–78%) in T:ET in grain-only wheat (Figures 3a, 3d and 3g). This is consistent with other studies (S. Kang et al., 2003; Wei et al., 2017; Zhou et al., 2016) that reported a very strong positive correlation between vegetation indices and T:ET. However, this relation was not strong for graze-grain and graze-out wheat systems (Figure 3). As each ET partitioning method has its inherent assumptions and associated limitations, similar evaluations were performed using periods for which ET partitioning estimates were available for all methods (Figure S5 in Supporting Information S1). These results also indicate

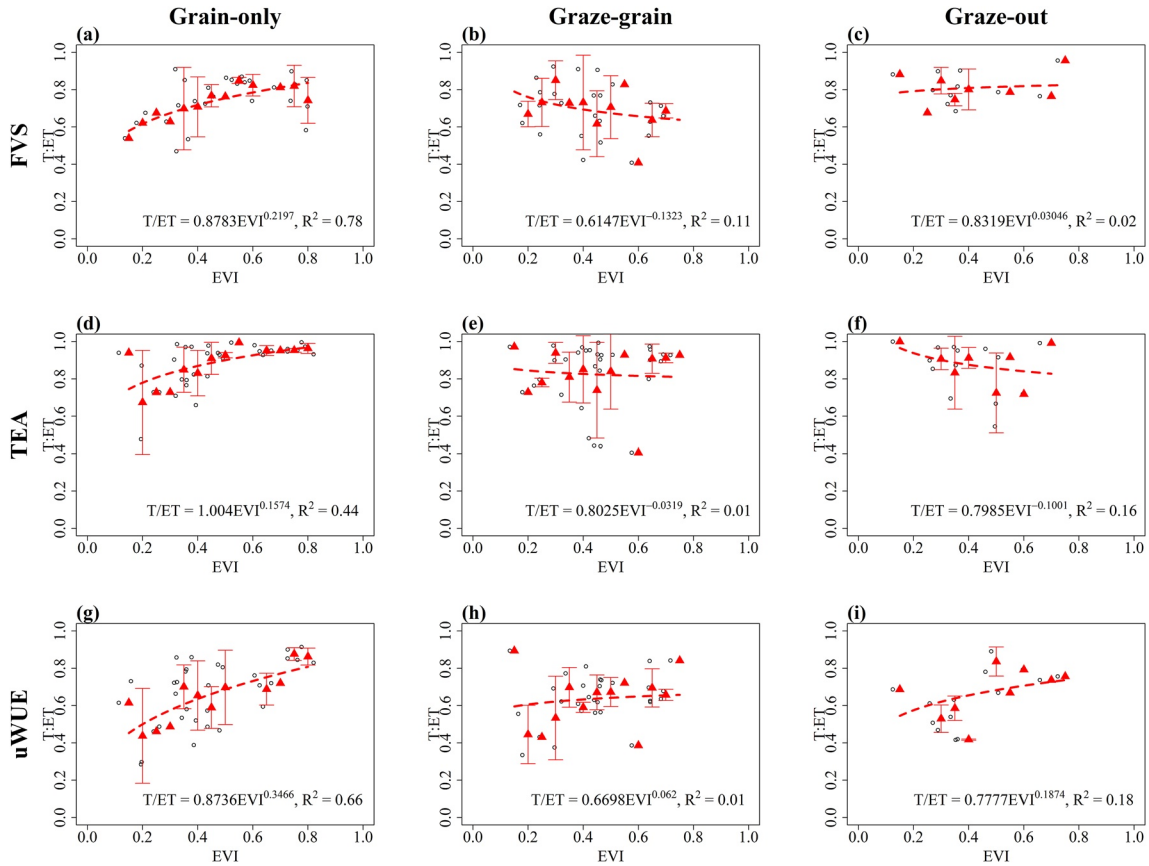

Figure 3. Relations between T:ET and enhanced vegetation index (EVI) in differently managed winter wheat systems using the three ET partitioning methods; (a–c) flux variance similarity, (d–f) transpiration estimation algorithm, and (g–i) underlying water use efficiency. Gray dots are weekly T:ET, ±3 days around the Landsat image acquisition date, during mid-day (11 a.m.–2 p.m.). Red triangles are averaged T:ET corresponding to 0.05-bin EVI. The vertical lines are the error bars of mean T:ET for each bin. The red dash line in each panel is the best nonlinear fit between triangles and corresponding EVI.

that T:ET-EVI relation was strong in grain-only wheat but this relation became weak for the grazed systems. In the following section, we explore this aspect in more detail.

3.3. Errors in the Prediction of T:ET Using EVI

The applicability of previously reported canonical relations between EVI and T:ET for crop systems was first assessed in both disturbed (i.e., grazed) and undisturbed (i.e., non-grazed) systems. To this end, the global crop relation ($T:ET = 0.66LAI^{0.18}$) presented in Wei et al. (2017) was used. LAI was obtained from EVI based on Y. Kang et al. (2016). Results (Figure 4d) show that Mean Absolute Percentage Error (MAPE) (see Text S2 in Supporting Information S1 for additional details regarding the calculation of MAPE) which was calculated using the predicted (i.e., T:ET obtained using the global crop relation (i.e., $T:ET = 0.66LAI^{0.18}$) of Wei et al. (2017) in different systems) and observed (i.e., T:ET obtained using FVS method) T:ET, was significantly worse for disturbed systems at both weekly and monthly scales. Notably, the errors are larger (Figures 4a–4c) even when the T:ET versus EVI relations derived at the neighboring undisturbed site (i.e., site corresponding to grain-only wheat system) is used from all the methods. For example, at weekly scale, MAPE was highest (about 20%) for graze-grain case and lowest (about 9%) for grain-only case for FVS-method (Figure 4a). Similar results were also observed at monthly scales, and for other partitioning methods. We also evaluated the errors in each wheat system when using T:ET-EVI relations obtained in a differently managed system (see Table 1). Errors generally increased, with a few exceptions, when the T:ET-EVI relation developed for a wheat system is used for other at both weekly and monthly scales. Although the three sites are all winter wheat systems that experience similar hydroclimatology, the difference in management implementations make them act differently in regards to T:ET dynamics vis-a-vis EVI. Among the different temporal scales, errors were minimum at the seasonal scale.

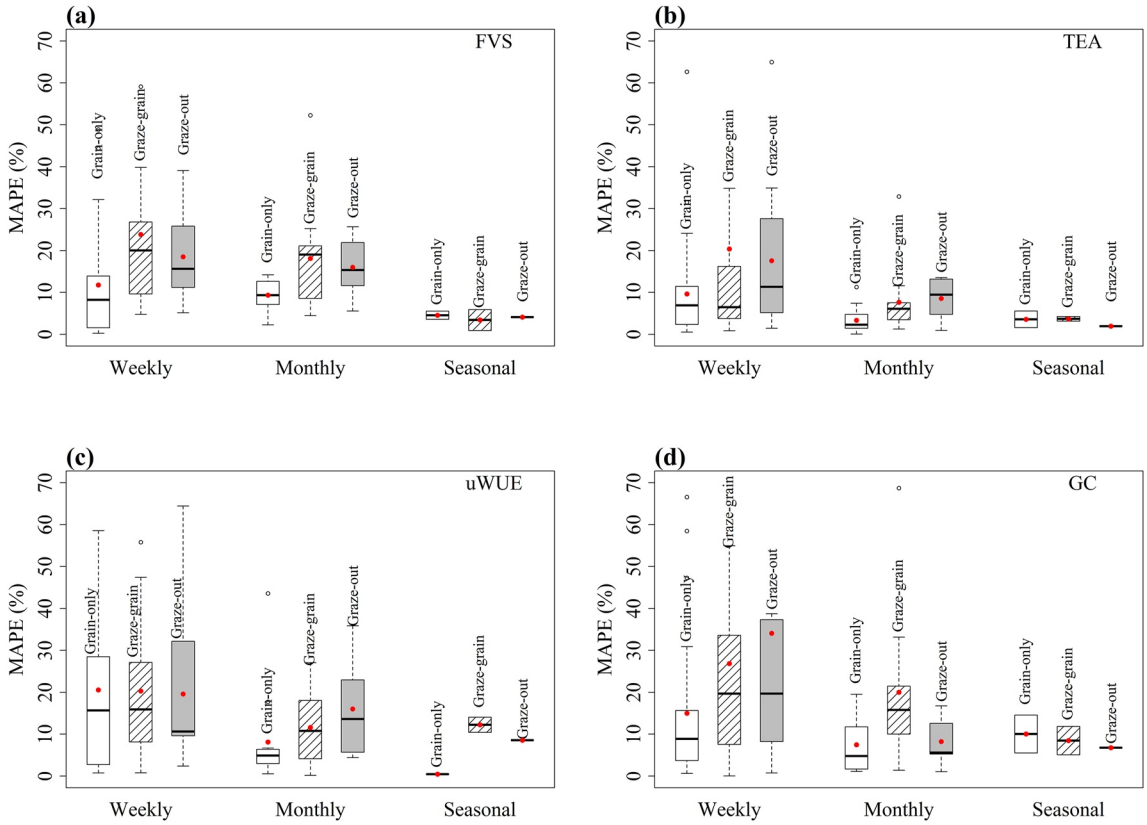

Figure 4. Mean absolute percentage error (MAPE) of predicted T:ET using the relations developed in unmanaged system from (a) flux variance similarity (FVS) method, (b) transpiration estimation algorithm method, and (c) underlying water use efficiency method at weekly, monthly, and seasonal time scales for winter wheat systems with varied management implementations. (d) An additional evaluation is performed using a relation (hereafter referred as GC) derived using global data over varied crops as presented in Wei et al. (2017). MAPE calculation in panels (a–c) used T:ET obtained using the respective partitioning method. In panel (d), T:ET were estimated using the FVS method. Red dots represent the average MAPE.

Table 1
Average Mean Absolute Percentage Error (%) When Using T:ET-Enhanced Vegetation Index Relations Obtained in Different Wheat Systems and the Global Crop Relation Presented in Wei et al. (2017)

	MAPE (%)								
	Weekly			Monthly			Seasonal		
T:ET-EVI relation	G	GG	GO	G	GG	GO	G	GG	GO
FVS (G)	11.76	23.84	18.50	9.33	18.12	16.01	4.55	3.42	4.09
FVS (GG)	20	17.67	12.1	15.97	15.53	9.23	2.61	2.04	2.67
FVS (GO)	19.16	32.54	8.96	8.36	20.91	7.92	15.43	13.55	12.75
TEA (G)	9.62	22.36	17.56	3.34	7.66	8.56	3.58	3.70	1.94
TEA (GG)	14.51	21.44	15.62	10.95	8.71	9.33	8.3	5.29	4.29
TEA (GO)	15.26	21.42	14.11	9.94	8.60	6.07	3.16	0.40	1.64
uWUE (G)	20.55	20.27	19.57	8.13	11.59	16.01	0.45	12.23	8.55
uWUE (GG)	27.65	30.13	26.58	29.54	26.98	30.87	29.61	27.54	26.97
uWUE (GO)	23.57	28.88	25.67	26.0	24.13	28.93	26.79	25.08	24.78
GC	14.99	26.84	34.06	7.46	20.00	8.24	10.04	8.47	6.77

Note. Here, G represents grain-only wheat system, GG represents graze-grain wheat system, GO represents graze-out wheat system, and GC represents the global crop relation.

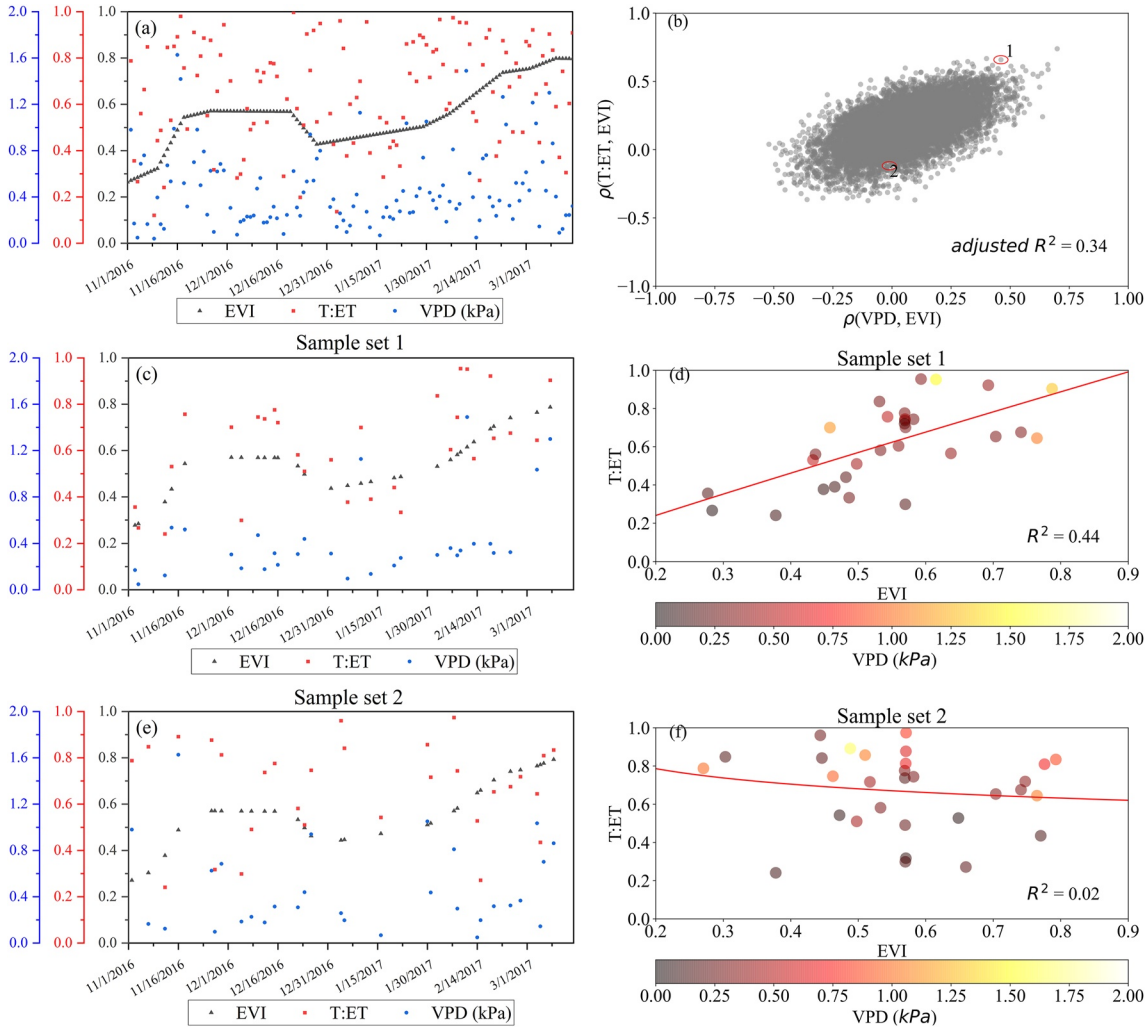

Figure 5. Temporal variations of enhanced vegetation index (EVI), flux variance similarity (FVS)-derived T:ET, and (a) vapor pressure deficit (VPD) for all days, (c) sample set 1, and (e) sample set 2. (b) Scatter of correlation between VPD and EVI and correlation between FVS-derived T:ET and EVI for 10,000 sample sets with each set having randomly selected 30 days. Scatter between FVS-derived T:ET and EVI for (d) sample set 1 and (f) sample set 2. Red solid lines in panels (d and f) represent the best-fit nonlinear lines.

Smaller error at the seasonal scale is consistent with other studies which reported that T:ET are uncorrelated with vegetation growth across sites (Fatichi & Pappas, 2017; Nelson et al., 2020).

We further investigated the possible causes for the lack of strong relation between T:ET and EVI in graze-grain and graze-out systems. At ecosystem-scale, T rate is controlled by meteorological conditions, the stomatal conductance (g_s), and plant's biophysical state (e.g., LAI, EVI, etc.). T is usually proportional to $g_s \times \text{LAI} \times \text{VPD}$. g_s is affected by multiple environmental variables, including VPD, soil moisture, radiation, and air temperature (Daly et al., 2004; Jarvis, 1976) (see Text S3 and Figure S11 in Supporting Information S1). Given our earlier result that showed a strong influence of VPD on T:ET (in Section 3.1), we started with a hypothesis that the increase in T:ET with EVI in undisturbed systems is strongly influenced by the covariation of VPD and EVI. Any disturbance or grazing management may, however, disturb the co-variation of EVI with VPD, thus also impacting the covariation of T:ET with EVI. To test this hypothesis, we obtained relations between EVI and T:ET for 10,000 different sample sets of randomly distributed 30 days from the growing season (Figure 5a) in the undisturbed system. Each set covers a wide enough range of EVI that is experienced in grain-only and graze-grain systems. The orientation of the point cloud along 1:1 direction in Figure 5b confirms that the relation between EVI and T:ET is stronger with higher correlation between VPD and EVI. To parse this further, we selected two sample sets with contrasting correlations between T:ET and EVI. Sample set 1 has ρ(T:ET, EVI) of 0.66 and sample set 2 has

ρ(T:ET, EVI) of −0.12. Here ρ is the coefficient of correlation. The results suggest that if EVI is not co-varying closely with VPD (sample set 2, see Figure 5e), then the relation between T:ET and EVI is not strong (Figure 5f). But if EVI co-varies closely with VPD, then the T:ET-EVI relation improves (see Figures 5c and 5d). In fact, at the unmanaged site where a strong T:ET-EVI relation is obtained (see Figure 1), the correlation between VPD and EVI until the peak growth period is 0.60. In contrast, the corresponding value for graze-grain and graze-out cases were 0.15 and −0.36, respectively. Similar evaluations were also conducted for uWUE (see Figure S9 in Supporting Information S1) method and TEA method (see Figure S10 in Supporting Information S1). The results in Figure 5, which are based on FVS-derived T:ET, also hold for the other methods (Figures S9 and S10 in Supporting Information S1). Furthermore, evaluations were also conducted for soil moisture, radiation, and air temperature, variables known to affect the stomatal conductance (see Figures S6–S8 in Supporting Information S1). Results indicate that the covariation of solar radiation with EVI also explained the covariation of T:ET with EVI, although the relation was less stronger. The influences of air temperature and soil moisture were much less (see Figures S7 and S8 in Supporting Information S1). These results indicate that the expressed T:ET-EVI relation works best with systems with a clear seasonal phenology, which usually results in improved correlation with VPD, provided VPD also exhibits an overall increasing trend during the growing season. When crop fields are grazed, plant development cycle or the phenology gets decoupled with the overall seasonal variation of VPD and radiation, thus limiting its explanatory power for seasonal T:ET variations. This is consistent with the reported poor explainability of T:ET by vegetation indices in grasslands and needle leaf forests (Zhou et al., 2016), that also lack distinct seasonal phenologies. Simulations based on a two-source ET model further corroborate the role of covariation between EVI and VPD on the strength of T:ET relation (see Text S4 and Figure S13 in Supporting Information S1). The two-source ET model elucidates the dependence of T:ET on both vegetation index and meteorological variables, including LAI (or EVI), VPD, solar radiation, soil moisture, etc. (see Equations 10a–10l in Supporting Information S1). Figures S14–S17 in Supporting Information S1 further highlight that T:ET is strongly affected by LAI (or EVI) variation, with it usually increasing with LAI. This is because a higher LAI (or EVI) leads to an increase in T. In addition, it also reduces E due to radiation shading and wind sheltering. However, given that T:ET is also dependent on solar radiation and VPD, the covariation of these variables with EVI within a season can alter the T:ET-EVI relation. Modification of EVI due to grazing during the growing season significantly alters the covariation of EVI and VPD or EVI and radiation, thus degrading the strength of T:ET-EVI relation. In fact, for many undisturbed sites, temporal variations of solar radiation, VPD, and/or soil moisture may lead to a weak T:ET-EVI relation.

4. Conclusions

Using T:ET-EVI relations, ET partitioning was performed in winter wheat systems with varied grazing management schemes. Comparison with partitioning estimates obtained based on three ET partitioning methods, viz. FVS theory, uWUE, and TEA, all indicate a robust T:ET-EVI relation in a standard undisturbed system. In contrast, the relation in disturbed systems, realized by cattle grazing in this case, is weak and does not capture the data variance well. The results indicate that the relation between vegetation indices and T:ET is affected by canopy alterations, which in this study was due to grazing management but could also be a result of other natural (e.g., fire or drought) or anthropogenic (e.g., thinning) disturbances. In addition, our results show prediction of T:ET at weekly to monthly scale using the T:ET-EVI relation of undisturbed systems in disturbed system introduces large errors. As prediction of T:ET using data from disturbed system in an undisturbed system and vice-versa introduces uncertainty in T:ET estimates, the results point to limited translatability of the method across systems. Given that more than 40% of the global land is managed or disturbed (Ellis et al., 2010), the results underscore the need for caution while assessing ET partitioning using vegetation indices over managed or disturbed systems. This is also relevant as many remote-sensing and land surface models formulate T:ET as a function of these plant development metrics (Lian et al., 2018; Miralles et al., 2016; Talsma et al., 2018). Notably, the impact of grazing management on T:ET estimate at the seasonal scale is negligible. This is attributable to plants' adaptation to the given water resources and the compensatory effects of E from wet canopies and wet soil surfaces under contrasting (dense and sparse) canopies.

Investigation on the possible causes of the altered T:ET-EVI relation suggests that grazing disturbed the co-variation of EVI and VPD (and of EVI and solar radiation), resulting in divergence from the standard T:ET-EVI relation. As the covariation between VPD (or solar radiation) and EVI can be easily evaluated using global

meteorological forcings (Mooney et al., 2011; Warszawski et al., 2014; Weedon et al., 2014; Xia et al., 2012) and vegetation (Benedetti & Rossini, 1993; Hatfield & Prueger, 2010; Huete et al., 1994, 2002; Jiang et al., 2008; Nguyen et al., 2020; Rocha & Shaver, 2009) data, future studies may use this metric, after further assessments in alternative settings, to map regions where vegetation indices are likely to be effective for ET partitioning.

Data Availability Statement

Authors thank developers of the Fluxpart source code, which is accessible at https://github.com/usda-ars-ussl/fluxpart (accessed on 10 November 2020). The code for TEA algorithm is available at https://doi.org/10.5281/zenodo.3921923. The code for uWUE algorithm is available at https://github.com/praghav444/WaterFlux-Partitioning. Data for this work are publicly available (Raghav et al., 2022, https://doi.org/10.15482/USDA.ADC/1527834)

Acknowledgments
This work is partially supported by NSF OIA-2019561, NSF EAR-1920425, and NSF EAR-1856054. Partial funding supports from the USDA-ARS Office of National Programs (Project number: 3070-21610-003-00D), USDA-ARS Long-Term Agroecosystem Research Network, and USDA-NIFA's research grant (Project No. 2019-68012-29888) are also acknowledged.

References

Alkama, R., & Cescatti, A. (2016). Biophysical climate impacts of recent changes in global forest cover. *Science*, *351*(6273), 600–604. https://doi.org/10.1126/science.aac8083

Bai, Y., Li, X., Zhou, S., Yang, X., Yu, K., Wang, M., et al. (2019). Quantifying plant transpiration and canopy conductance using eddy flux data: An underlying water use efficiency method. *Agricultural and Forest Meteorology*, *271*, 375–384. https://doi.org/10.1016/j.agrformet.2019.02.035

Bates, D. M., & Watts, D. G. (1988). *Nonlinear regression analysis and its applications* (Vol. 2). Wiley.

Benedetti, R., & Rossini, P. (1993). On the use of NDVI profiles as a tool for agricultural statistics: The case study of wheat yield estimate and forecast in Emilia Romagna. *Remote Sensing of Environment*, *45*(3), 311–326. https://doi.org/10.1016/0034-4257(93)90113-c

Berkelhammer, M., Noone, D., Wong, T., Burns, S., Knowles, J., Kaushik, A., et al. (2016). Convergent approaches to determine an ecosystem's transpiration fraction. *Global Biogeochemical Cycles*, *30*(6), 933–951. https://doi.org/10.1002/2016gb005392

Black, T., Gardner, W., & Thurtell, G. (1969). The prediction of evaporation, drainage, and soil water storage for a bare soil. *Soil Science Society of America Journal*, *33*(5), 655–660. https://doi.org/10.2136/sssaj1969.03615995003300050013x

Bonetti, S., Manoli, G., Domec, J.-C., Putti, M., Marani, M., & Katul, G. G. (2015). The influence of water table depth and the free atmospheric state on convective rainfall predisposition. *Water Resources Research*, *51*(4), 2283–2297. https://doi.org/10.1002/2014wr016431

Brutsaert, W. (2013). Evaporation into the atmosphere: Theory. In *History and applications* (Vol. 1). Springer Science & Business Media.

Cammalleri, C., Rallo, G., Agnese, C., Ciraolo, G., Minacapilli, M., & Provenzano, G. (2013). Combined use of eddy covariance and sap flow techniques for partition of ET fluxes and water stress assessment in an irrigated olive orchard. *Agricultural Water Management*, *120*, 89–97. https://doi.org/10.1016/j.agwat.2012.10.003

Chen, S., Billings, S. A., & Luo, W. (1989). Orthogonal least squares methods and their application to non-linear system identification. *International Journal of Control*, *50*(5), 1873–1896. https://doi.org/10.1080/00207178908953472

Chen, X., Kumar, M., & McGlynn, B. L. (2015). Variations in streamflow response to large hurricane-season storms in a southeastern US watershed. *Journal of Hydrometeorology*, *16*(1), 55–69. https://doi.org/10.1175/jhm-d-14-0044.1

Condon, L. E., & Maxwell, R. M. (2019). Simulating the sensitivity of evapotranspiration and streamflow to large-scale groundwater depletion. *Science Advances*, *5*(6), eaav4574. https://doi.org/10.1126/sciadv.aav4574

Daly, E., Porporato, A., & Rodriguez-Iturbe, I. (2004). Coupled dynamics of photosynthesis, transpiration, and soil water balance. Part I: Upscaling from hourly to daily level. *Journal of Hydrometeorology*, *5*(3), 546–558. https://doi.org/10.1175/1525-7541(2004)005<0546:cdopta>2.0.co;2

Dirmeyer, P. A., Gao, X., Zhao, M., Guo, Z., Oki, T., & Hanasaki, N. (2006). GSWP-2: Multimodel analysis and implications for our perception of the land surface. *Bulletin of the American Meteorological Society*, *87*(10), 1381–1398. https://doi.org/10.1175/bams-87-10-1381

Ellis, E. C., Klein Goldewijk, K., Siebert, S., Lightman, D., & Ramankutty, N. (2010). Anthropogenic transformation of the biomes, 1700 to 2000. *Global Ecology and Biogeography*, *19*(5), 589–606. https://doi.org/10.1111/j.1466-8238.2010.00540.x

Elzhov. T. V., Mullen, K. M., Spiess, A., & Bolker, B. (2010). R interface to the Levenberg-Marquardt nonlinear least-squares algorithm found in MINPACK, plus support for bounds. *R package version 1.1-8*. http://cran.r-project.org/package=minpack.lm

Fatichi, S., & Pappas, C. (2017). Constrained variability of modeled T: ET ratio across biomes. *Geophysical Research Letters*, *44*(13), 6795–6803. https://doi.org/10.1002/2017gl074041

Ferretti, D., Pendall, E., Morgan, J., Nelson, J., Lecain, D., & Mosier, A. (2003). Partitioning evapotranspiration fluxes from a Colorado grassland using stable isotopes: Seasonal variations and ecosystem implications of elevated atmospheric CO_2. *Plant and Soil*, *254*(2), 291–303. https://doi.org/10.1023/a:1025511618571

Good, S. P., Moore, G. W., & Miralles, D. G. (2017). A mesic maximum in biological water use demarcates biome sensitivity to aridity shifts. *Nature Ecology & Evolution*, *1*(12), 1883–1888. https://doi.org/10.1038/s41559-017-0371-8

Good, S. P., Noone, D., & Bowen, G. (2015). Hydrologic connectivity constrains partitioning of global terrestrial water fluxes. *Science*, *349*(6244), 175–177. https://doi.org/10.1126/science.aaa5931

Haddeland, I., Clark, D. B., Franssen, W., Ludwig, F., Voß, F., Arnell, N. W., et al. (2011). Multimodel estimate of the global terrestrial water balance: Setup and first results. *Journal of Hydrometeorology*, *12*(5), 869–884. https://doi.org/10.1175/2011jhm1324.1

Hatfield, J. L., & Prueger, J. H. (2010). Value of using different vegetative indices to quantify agricultural crop characteristics at different growth stages under varying management practices. *Remote Sensing*, *2*(2), 562–578. https://doi.org/10.3390/rs2020562

Hu, H., Chen, L., Liu, H., Ali Khan, M. Y., Tie, Q., Zhang, X., & Tian, F. (2018). Comparison of the vegetation effect on ET partitioning based on eddy covariance method at five different sites of northern China. *Remote Sensing*, *10*(11), 1755. https://doi.org/10.3390/rs10111755

Hu, X., & Lei, H. (2021). Evapotranspiration partitioning and its interannual variability over a winter wheat-summer maize rotation system in the North China Plain. *Agricultural and Forest Meteorology*, *310*, 108635. https://doi.org/10.1016/j.agrformet.2021.108635

Huete, A., Didan, K., Miura, T., Rodriguez, E. P., Gao, X., & Ferreira, L. G. (2002). Overview of the radiometric and biophysical performance of the MODIS vegetation indices. *Remote Sensing of Environment*, *83*(1–2), 195–213. https://doi.org/10.1016/s0034-4257(02)00096-2

Huete, A., Justice, C., & Liu, H. (1994). Development of vegetation and soil indices for MODIS-EOS. *Remote Sensing of Environment*, *49*(3), 224–234. https://doi.org/10.1016/0034-4257(94)90018-3

Jarvis, P. (1976). The interpretation of the variations in leaf water potential and stomatal conductance found in canopies in the field. *Philosophical Transactions of the Royal Society of London B Biological Sciences*, *273*(927), 593–610.
Jasechko, S., Sharp, Z. D., Gibson, J. J., Birks, S. J., Yi, Y., & Fawcett, P. J. (2013). Terrestrial water fluxes dominated by transpiration. *Nature*, *496*(7445), 347–350. https://doi.org/10.1038/nature11983
Jiang, Z., Huete, A. R., Didan, K., & Miura, T. (2008). Development of a two-band enhanced vegetation index without a blue band. *Remote Sensing of Environment*, *112*(10), 3833–3845. https://doi.org/10.1016/j.rse.2008.06.006
Jung, M., Reichstein, M., Ciais, P., Seneviratne, S. I., Sheffield, J., Goulden, M. L., et al. (2010). Recent decline in the global land evapotranspiration trend due to limited moisture supply. *Nature*, *467*(7318), 951–954. https://doi.org/10.1038/nature09396
Kang, S., Gu, B., Du, T., & Zhang, J. (2003). Crop coefficient and ratio of transpiration to evapotranspiration of winter wheat and maize in a semi-humid region. *Agricultural Water Management*, *59*(3), 239–254. https://doi.org/10.1016/s0378-3774(02)00150-6
Kang, Y., Özdoğan, M., Zipper, S. C., Román, M. O., Walker, J., Hong, S. Y., et al. (2016). How universal is the relationship between remotely sensed vegetation indices and crop leaf area index? A global assessment. *Remote Sensing*, *8*(7), 597. https://doi.org/10.3390/rs8070597
Kim, S.-H., Sicher, R. C., Bae, H., Gitz, D. C., Baker, J. T., Timlin, D. J., & Reddy, V. R. (2006). Canopy photosynthesis, evapotranspiration, leaf nitrogen, and transcription profiles of maize in response to CO_2 enrichment. *Global Change Biology*, *12*(3), 588–600. https://doi.org/10.1111/j.1365-2486.2006.01110.x
Kool, D., Agam, N., Lazarovitch, N., Heitman, J., Sauer, T., & Ben-Gal, A. (2014). A review of approaches for evapotranspiration partitioning. *Agricultural and Forest Meteorology*, *184*, 56–70. https://doi.org/10.1016/j.agrformet.2013.09.003
Li, X., Gentine, P., Lin, C., Zhou, S., Sun, Z., Zheng, Y., et al. (2019). A simple and objective method to partition evapotranspiration into transpiration and evaporation at eddy-covariance sites. *Agricultural and Forest Meteorology*, *265*, 171–182. https://doi.org/10.1016/j.agrformet.2018.11.017
Lian, X., Piao, S., Huntingford, C., Li, Y., Zeng, Z., Wang, X., et al. (2018). Partitioning global land evapotranspiration using CMIP5 models constrained by observations. *Nature Climate Change*, *8*(7), 640–646. https://doi.org/10.1038/s41558-018-0207-9
Liu, C., Zhang, X., & Zhang, Y. (2002). Determination of daily evaporation and evapotranspiration of winter wheat and maize by large-scale weighing lysimeter and micro-lysimeter. *Agricultural and Forest Meteorology*, *111*(2), 109–120. https://doi.org/10.1016/s0168-1923(02)00015-1
Liu, Y., Kumar, M., Katul, G. G., Feng, X., & Konings, A. G. (2020). Plant hydraulics accentuates the effect of atmospheric moisture stress on transpiration. *Nature Climate Change*, *10*(7), 691–695. https://doi.org/10.1038/s41558-020-0781-5
Liu, Y., Parolari, A. J., Kumar, M., Huang, C.-W., Katul, G. G., & Porporato, A. (2017). Increasing atmospheric humidity and CO_2 concentration alleviate forest mortality risk. *Proceedings of the National Academy of Sciences of the United States of America*, *114*(37), 9918–9923. https://doi.org/10.1073/pnas.1704811114
Long, D., & Singh, V. P. (2012). A two-source trapezoid model for evapotranspiration (TTME) from satellite imagery. *Remote Sensing of Environment*, *121*, 370–388. https://doi.org/10.1016/j.rse.2012.02.015
Ma, Y., & Song, X. (2019). Applying stable isotopes to determine seasonal variability in evapotranspiration partitioning of winter wheat for optimizing agricultural management practices. *Science of the Total Environment*, *654*, 633–642. https://doi.org/10.1016/j.scitotenv.2018.11.176
Martens, B., Miralles, D. G., Lievens, H., Van Der Schalie, R., De Jeu, R. A., Fernández-Prieto, D., et al. (2017). GLEAM v3: Satellite-based land evaporation and root-zone soil moisture. *Geoscientific Model Development*, *10*(5), 1903–1925. https://doi.org/10.5194/gmd-10-1903-2017
Massman, W. (1998). A review of the molecular diffusivities of H_2O, CO_2, CH_4, CO, O_3, SO_2, NH_3, N_2O, NO, and NO_2 in air, O_2 and N_2 near STP. *Atmospheric Environment*, *32*(6), 1111–1127. https://doi.org/10.1016/s1352-2310(97)00391-9
Migliavacca, M., Musavi, T., Mahecha, M. D., Nelson, J. A., Knauer, J., Baldocchi, D. D., et al. (2021). The three major axes of terrestrial ecosystem function. *Nature*, *598*(7881), 468–472. https://doi.org/10.1038/s41586-021-03939-9
Miralles, D. G., Holmes, T., De Jeu, R., Gash, J., Meesters, A., & Dolman, A. (2011). Global land-surface evaporation estimated from satellite-based observations. *Hydrology and Earth System Sciences*, *15*(2), 453–469. https://doi.org/10.5194/hess-15-453-2011
Miralles, D. G., Jiménez, C., Jung, M., Michel, D., Ershadi, A., McCabe, M., et al. (2016). The WACMOS-ET project–Part 2: Evaluation of global terrestrial evaporation data sets. *Hydrology and Earth System Sciences*, *20*(2), 823–842. https://doi.org/10.5194/hess-20-823-2016
Mooney, P. A., Mulligan, F. J., & Fealy, R. (2011). Comparison of ERA-40, ERA-Interim and NCEP/NCAR reanalysis data with observed surface air temperatures over Ireland. *International Journal of Climatology*, *31*(4), 545–557. https://doi.org/10.1002/joc.2098
Nelson, J. A., Carvalhais, N., Cuntz, M., Delpierre, N., Knauer, J., Ogée, J., et al. (2018). Coupling water and carbon fluxes to constrain estimates of transpiration: The TEA algorithm. *Journal of Geophysical Research: Biogeosciences*, *123*(12), 3617–3632. https://doi.org/10.1029/2018jg004727
Nelson, J. A., Pérez-Priego, O., Zhou, S., Poyatos, R., Zhang, Y., Blanken, P. D., et al. (2020). Ecosystem transpiration and evaporation: Insights from three water flux partitioning methods across FLUXNET sites. *Global Change Biology*, *26*(12), 6916–6930. https://doi.org/10.1111/gcb.15314
Nguyen, L. H., Joshi, D. R., Clay, D. E., & Henebry, G. M. (2020). Characterizing land cover/land use from multiple years of and sat and MODIS time series: A novel approach using land surface phenology modeling and random forest classifier. *Remote Sensing of Environment*, *238*, 111017. https://doi.org/10.1016/j.rse.2018.12.016
Oishi, A. C., Oren, R., Novick, K. A., Palmroth, S., & Katul, G. G. (2010). Interannual invariability of forest evapotranspiration and its consequence to water flow downstream. *Ecosystems*, *13*(3), 421–436. https://doi.org/10.1007/s10021-010-9328-3
Oki, T., & Kanae, S. (2006). Global hydrological cycles and world water resources. *Science*, *313*(5790), 1068–1072. https://doi.org/10.1126/science.1128845
Palatella, L., Rana, G., & Vitale, D. (2014). Towards a flux-partitioning procedure based on the direct use of high-frequency eddy-covariance data. *Boundary-Layer Meteorology*, *153*(2), 327–337. https://doi.org/10.1007/s10546-014-9947-x
Paschalis, A., Fatichi, S., Pappas, C., & Or, D. (2018). Covariation of vegetation and climate constrains present and future T/ET variability. *Environmental Research Letters*, *13*(10), 104012. https://doi.org/10.1088/1748-9326/aae267
Paul-Limoges, E., Wolf, S., Schneider, F. D., Longo, M., Moorcroft, P., Gharun, M., & Damm, A. (2020). Partitioning evapotranspiration with concurrent eddy covariance measurements in a mixed forest. *Agricultural and Forest Meteorology*, *280*, 107786. https://doi.org/10.1016/j.agrformet.2019.107786
Peddinti, S. R., & Kambhammettu, B. P. (2019). Dynamics of crop coefficients for citrus orchards of central India using water balance and eddy covariance flux partition techniques. *Agricultural Water Management*, *212*, 68–77. https://doi.org/10.1016/j.agwat.2018.08.027
Perez-Priego, O., Katul, G., Reichstein, M., El-Madany, T. S., Ahrens, B., Carrara, A., et al. (2018). Partitioning eddy covariance water flux components using physiological and micrometeorological approaches. *Journal of Geophysical Research: Biogeosciences*, *123*(10), 3353–3370. https://doi.org/10.1029/2018jg004637
Raghav, P., & Kumar, M. (2021). Retrieving gap-free daily root zone soil moisture using surface flux equilibrium theory. *Environmental Research Letters*, *16*(10), 104007. https://doi.org/10.1088/1748-9326/ac2441

Raghav, P., Wagle, P., Kumar, M., Banerjee, T., & Neel, J. P. S. (2022). Data from: Vegetation index-based partitioning of evapotranspiration is deficient in grazed systems. Ag Data Commons. https://doi.org/10.15482/USDA.ADC/1527834

Rana, G., Palatella, L., Scanlon, T. M., Martinelli, N., & Ferrara, R. M. (2018). CO_2 and H_2O flux partitioning in a Mediterranean cropping system. *Agricultural and Forest Meteorology*, *260*, 118–130. https://doi.org/10.1016/j.agrformet.2018.06.007

Räsänen, M., Aurela, M., Vakkari, V., Beukes, J. P., Tuovinen, J.-P., Van Zyl, P. G., et al. (2020). The effect of rainfall amount and timing on annual transpiration in grazed savanna grassland. *Hydrology and Earth System Sciences Discussions*, 1–31. https://doi.org/10.5194/hess-2019-651

Reichstein, M., Falge, E., Baldocchi, D., Papale, D., Aubinet, M., Berbigier, P., et al. (2005). On the separation of net ecosystem exchange into assimilation and ecosystem respiration: Review and improved algorithm. *Global Change Biology*, *11*(9), 1424–1439. https://doi.org/10.1111/j.1365-2486.2005.001002.x

Ritchie, J. T., & Burnett, E. (1971). Dryland evaporative flux in a subhumid climate: II. Plant influences 1. *Agronomy Journal*, *63*(1), 56–62. https://doi.org/10.2134/agronj1971.00021962006300010019x

Rocha, A. V., & Shaver, G. R. (2009). Advantages of a two band EVI calculated from solar and photosynthetically active radiation fluxes. *Agricultural and Forest Meteorology*, *149*(9), 1560–1563. https://doi.org/10.1016/j.agrformet.2009.03.016

Scanlon, T. M., & Kustas, W. P. (2010). Partitioning carbon dioxide and water vapor fluxes using correlation analysis. *Agricultural and Forest Meteorology*, *150*(1), 89–99. https://doi.org/10.1016/j.agrformet.2009.09.005

Scanlon, T. M., & Kustas, W. P. (2012). Partitioning evapotranspiration using an eddy covariance-based technique: Improved assessment of soil moisture and land–atmosphere exchange dynamics. *Vadose Zone Journal*, *11*(3), vzj2012.0025. https://doi.org/10.2136/vzj2012.0025

Scanlon, T. M., & Sahu, P. (2008). On the correlation structure of water vapor and carbon dioxide in the atmospheric surface layer: A basis for flux partitioning. *Water Resources Research*, *44*(10), W10418. https://doi.org/10.1029/2008wr006932

Scanlon, T. M., Schmidt, D. F., & Skaggs, T. H. (2019). Correlation-based flux partitioning of water vapor and carbon dioxide fluxes: Method simplification and estimation of canopy water use efficiency. *Agricultural and Forest Meteorology*, *279*, 107732. https://doi.org/10.1016/j.agrformet.2019.107732

Scott, R. L., & Biederman, J. A. (2017). Partitioning evapotranspiration using long-term carbon dioxide and water vapor fluxes. *Geophysical Research Letters*, *44*(13), 6833–6840. https://doi.org/10.1002/2017gl074324

Sinclair, T. R., Tanner, C., & Bennett, J. (1984). Water-use efficiency in crop production. *BioScience*, *34*(1), 36–40. https://doi.org/10.2307/1309424

Skaggs, T. H., Anderson, R. G., Alfieri, J., Scanlon, T., & Kustas, W. (2018). Fluxpart: Open source software for partitioning carbon dioxide and water vapor fluxes. *Agricultural and Forest Meteorology*, *253*, 218–224. https://doi.org/10.1016/j.agrformet.2018.02.019

Stoy, P. C., El-Madany, T. S., Fisher, J. B., Gentine, P., Gerken, T., Good, S. P., et al. (2019). Reviews and syntheses: Turning the challenges of partitioning ecosystem evaporation and transpiration into opportunities. *Biogeosciences*, *16*(19), 3747–3775. https://doi.org/10.5194/bg-16-3747-2019

Sulman, B. N., Roman, D. T., Scanlon, T. M., Wang, L., & Novick, K. A. (2016). Comparing methods for partitioning a decade of carbon dioxide and water vapor fluxes in a temperate forest. *Agricultural and Forest Meteorology*, *226*, 229–245. https://doi.org/10.1016/j.agrformet.2016.06.002

Sun, J.-Y., Sun, X.-Y., Hu, Z.-Y., & Wang, G.-X. (2020). Exploring the influence of environmental factors in partitioning evapotranspiration along an elevation gradient on Mount Gongga, eastern edge of the Qinghai-Tibet Platea, China. *Journal of Mountain Science*, *17*(2), 384–396. https://doi.org/10.1007/s11629-019-5687-1

Sun, X., Wilcox, B. P., & Zou, C. B. (2019). Evapotranspiration partitioning in dryland ecosystems: A global meta-analysis of in situ studies. *Journal of Hydrology*, *576*, 123–136. https://doi.org/10.1016/j.jhydrol.2019.06.022

Talsma, C. J., Good, S. P., Jimenez, C., Martens, B., Fisher, J. B., Miralles, D. G., et al. (2018). Partitioning of evapotranspiration in remote sensing-based models. *Agricultural and Forest Meteorology*, *260*, 131–143. https://doi.org/10.1016/j.agrformet.2018.05.010

Unkovich, M., Baldock, J., & Farquharson, R. (2018). Field measurements of bare soil evaporation and crop transpiration, and transpiration efficiency, for rainfed grain crops in Australia–a review. *Agricultural Water Management*, *205*, 72–80. https://doi.org/10.1016/j.agwat.2018.04.016

Wagle, P., Gowda, P. H., Manjunatha, P., Northup, B. K., Rocateli, A. C., & Taghvaeian, S. (2019). Carbon and water dynamics in co-located winter wheat and canola fields in the US Southern Great Plains. *Agricultural and Forest Meteorology*, *279*, 107714. https://doi.org/10.1016/j.agrformet.2019.107714

Wagle, P., Gowda, P. H., Northup, B. K., & Neel, J. P. (2021). Ecosystem-level water use efficiency and evapotranspiration partitioning in conventional till and no-till rainfed canola. *Agricultural Water Management*, *250*, 106825. https://doi.org/10.1016/j.agwat.2021.106825

Wagle, P., Gowda, P. H., Northup, B. K., Turner, K. E., Neel, J. P., Manjunatha, P., & Zhou, Y. (2018). Variability in carbon dioxide fluxes among six winter wheat paddocks managed under different tillage and grazing practices. *Atmospheric Environment*, *185*, 100–108. https://doi.org/10.1016/j.atmosenv.2018.05.003

Wagle, P., Skaggs, T. H., Gowda, P. H., Northup, B. K., & Neel, J. P. (2020). Flux variance similarity-based partitioning of evapotranspiration over a rainfed alfalfa field using high frequency eddy covariance data. *Agricultural and Forest Meteorology*, *285*, 107907. https://doi.org/10.1016/j.agrformet.2020.107907

Wagle, P., Skaggs, T. H., Gowda, P. H., Northup, B. K., Neel, J. P., & Anderson, R. G. (2021). Evaluation of water use efficiency algorithms for flux variance similarity-based evapotranspiration partitioning in C3 and C4 grain crops. *Water Resources Research*, *57*(5), e2020WR028866. https://doi.org/10.1029/2020WR028866

Wang, H., & Liu, C. (2007). Soil evaporation and its affecting factors under crop canopy. *Communications in Soil Science and Plant Analysis*, *38*(1–2), 259–271. https://doi.org/10.1080/00103620601094213

Wang, L., Caylor, K. K., Villegas, J. C., Barron-Gafford, G. A., Breshears, D. D., & Huxman, T. E. (2010). Partitioning evapotranspiration across gradients of woody plant cover: Assessment of a stable isotope technique. *Geophysical Research Letters*, *37*(9), L09401. https://doi.org/10.1029/2010gl043228

Wang, L., Good, S. P., & Caylor, K. K. (2014). Global synthesis of vegetation control on evapotranspiration partitioning. *Geophysical Research Letters*, *41*(19), 6753–6757. https://doi.org/10.1002/2014gl061439

Wang, R., Kumar, M., & Marks, D. (2013). Anomalous trend in soil evaporation in a semi-arid, snow-dominated watershed. *Advances in Water Resources*, *57*, 32–40. https://doi.org/10.1016/j.advwatres.2013.03.004

Wang, W., Smith, J. A., Ramamurthy, P., Baeck, M. L., Bou-Zeid, E., & Scanlon, T. M. (2016). On the correlation of water vapor and CO_2: Application to flux partitioning of evapotranspiration. *Water Resources Research*, *52*(12), 9452–9469. https://doi.org/10.1002/2015wr018161

Warszawski, L., Frieler, K., Huber, V., Piontek, F., Serdeczny, O., & Schewe, J. (2014). The inter-sectoral impact model intercomparison project (ISI–MIP): Project framework. *Proceedings of the National Academy of Sciences of the United States of America*, *111*(9), 3228–3232. https://doi.org/10.1073/pnas.1312330110

Weedon, G. P., Balsamo, G., Bellouin, N., Gomes, S., Best, M. J., & Viterbo, P. (2014). The WFDEI meteorological forcing data set: WATCH forcing data methodology applied to ERA-interim reanalysis data. *Water Resources Research*, *50*(9), 7505–7514. https://doi.org/10.1002/2014wr015638

Wei, Z., Yoshimura, K., Okazaki, A., Kim, W., Liu, Z., & Yokoi, M. (2015). Partitioning of evapotranspiration using high-frequency water vapor isotopic measurement over a rice paddy field. *Water Resources Research*, *51*(5), 3716–3729. https://doi.org/10.1002/2014wr016737

Wei, Z., Yoshimura, K., Wang, L., Miralles, D. G., Jasechko, S., & Lee, X. (2017). Revisiting the contribution of transpiration to global terrestrial evapotranspiration. *Geophysical Research Letters*, *44*(6), 2792–2801. https://doi.org/10.1002/2016gl072235

Williams, D., Cable, W., Hultine, K., Hoedjes, J., Yepez, E., Simonneaux, V., et al. (2004). Evapotranspiration components determined by stable isotope, sap flow and eddy covariance techniques. *Agricultural and Forest Meteorology*, *125*(3–4), 241–258. https://doi.org/10.1016/j.agrformet.2004.04.008

Wutzler, T., Lucas-Moffat, A., Migliavacca, M., Knauer, J., Sickel, K., Šigut, L., et al. (2018). Basic and extensible post-processing of eddy covariance flux data with REddyProc. *Biogeosciences*, *15*(16), 5015–5030. https://doi.org/10.5194/bg-15-5015-2018

Xia, Y., Mitchell, K., Ek, M., Cosgrove, B., Sheffield, J., Luo, L., et al. (2012). Continental-scale water and energy flux analysis and validation for North American Land Data Assimilation Ssystem project phase 2 (NLDAS-2): 2. Validation of model-simulated streamflow. *Journal of Geophysical Research*, *117*(D3), D03110. https://doi.org/10.1029/2011jd016051

Xiao, W., Wei, Z., & Wen, X. (2018). Evapotranspiration partitioning at the ecosystem scale using the stable isotope method—A review. *Agricultural and Forest Meteorology*, *263*, 346–361. https://doi.org/10.1016/j.agrformet.2018.09.005

Xu, Z., Zhu, Z., Liu, S., Song, L., Wang, X., Zhou, S., et al. (2021). Evapotranspiration partitioning for multiple ecosystems within a dryland watershed: Seasonal variations and controlling factors. *Journal of Hydrology*, *598*, 126483. https://doi.org/10.1016/j.jhydrol.2021.126483

Yaseef, N. R., Yakir, D., Rotenberg, E., Schiller, G., & Cohen, S. (2010). Ecohydrology of a semi-arid forest: Partitioning among water balance components and its implications for predicted precipitation changes. *Ecohydrology: Ecosystems, Land and Water Process Interactions, Ecohydrogeomorphology*, *3*(2), 143–154. https://doi.org/10.1002/eco.65

Yu, L.-P., Huang, G.-H., Liu, H.-J., Wang, X.-P., & Wang, M.-Q. (2009). Experimental investigation of soil evaporation and evapotranspiration of winter wheat under sprinkler irrigation. *Agricultural Sciences in China*, *8*(11), 1360–1368. https://doi.org/10.1016/s1671-2927(08)60348-x

Zeng, Z., Piao, S., Li, L. Z., Zhou, L., Ciais, P., Wang, T., et al. (2017). Climate mitigation from vegetation biophysical feedbacks during the past three decades. *Nature Climate Change*, *7*(6), 432–436. https://doi.org/10.1038/nclimate3299

Zhang, Y., Kong, D., Gan, R., Chiew, F. H., McVicar, T. R., Zhang, Q., & Yang, Y. (2019). Coupled estimation of 500 m and 8-day resolution global evapotranspiration and gross primary production in 2002–2017. *Remote Sensing of Environment*, *222*, 165–182. https://doi.org/10.1016/j.rse.2018.12.031

Zhang, Y., Peña-Arancibia, J. L., McVicar, T. R., Chiew, F. H., Vaze, J., Liu, C., et al. (2016). Multi-decadal trends in global terrestrial evapotranspiration and its components. *Scientific Reports*, *6*(1), 1–12. https://doi.org/10.1038/srep19124

Zhou, S., Yu, B., Huang, Y., & Wang, G. (2014). The effect of vapor pressure deficit on water use efficiency at the subdaily time scale. *Geophysical Research Letters*, *41*(14), 5005–5013. https://doi.org/10.1002/2014gl060741

Zhou, S., Yu, B., Zhang, Y., Huang, Y., & Wang, G. (2016). Partitioning evapotranspiration based on the concept of underlying water use efficiency. *Water Resources Research*, *52*(2), 1160–1175. https://doi.org/10.1002/2015wr017766

Zhou, S., Yu, B., Zhang, Y., Huang, Y., & Wang, G. (2018). Water use efficiency and evapotranspiration partitioning for three typical ecosystems in the Heihe River Basin, northwestern China. *Agricultural and Forest Meteorology*, *253*, 261–273. https://doi.org/10.1016/j.agrformet.2018.02.002

References From the Supporting Information

Bink, N., & Meesters, A. (1997). Comment on 'Estimation of surface heat and momentum fluxes using the flux-variance method above uniform and non-uniform terrain' by Katul et al.(1995). *Boundary-Layer Meteorology*, *84*(3), 497–502. https://doi.org/10.1023/a:1000427431944

Campbell, G. S., & Norman, J. (2012). *An introduction to environmental biophysics*. Springer Science & Business Media.

Hill, R. J. (1989). Implications of Monin–Obukhov similarity theory for scalar quantities. *Journal of the Atmospheric Sciences*, *46*(14), 2236–2244. https://doi.org/10.1175/1520-0469(1989)046<2236:iomstf>2.0.co;2

Katul, G. G., & Parlange, M. B. (1995). Analysis of land surface heat fluxes using the orthonormal wavelet approach. *Water Resources Research*, *31*(11), 2743–2749. https://doi.org/10.1029/95wr00003

Monin, A. S., & Obukhov, A. M. (1954). Basic laws of turbulent mixing in the surface layer of the atmosphere. *Contrib. Geophys. Inst. Acad. Sci. USSR*, *151*(163), e187.

Monteith, J. L. (1965). *Evaporation and environment* (pp. 205–234). Cambridge University Press (CUP).

Ronda, R., De Bruin, H., & Holtslag, A. (2001). Representation of the canopy conductance in modeling the surface energy budget for low vegetation. *Journal of Applied Meteorology*, *40*(8), 1431–1444. https://doi.org/10.1175/1520-0450(2001)040<1431:rotcci>2.0.co;2

Sellers, P. J., Heiser, M. D., & Hall, F. G. (1992). Relations between surface conductance and spectral vegetation indices at intermediate (100 m^2 to 15 km^2) length scales. *Journal of Geophysical Research*, *97*(D17), 19033–19059. https://doi.org/10.1029/92jd01096

Shuttleworth, W. J., & Gurney, R. J. (1990). The theoretical relationship between foliage temperature and canopy resistance in sparse crops. *Quarterly Journal of the Royal Meteorological Society*, *116*(492), 497–519. https://doi.org/10.1002/qj.49711649213

Shuttleworth, W. J., & Wallace, J. (1985). Evaporation from sparse crops-an energy combination theory. *Quarterly Journal of the Royal Meteorological Society*, *111*(469), 839–855. https://doi.org/10.1002/qj.49711146910

Supplementary Information for

"Vegetation index-based partitioning of evapotranspiration is deficient in grazed systems"

Pushpendra Raghav[1], Pradeep Wagle[2], Mukesh Kumar[1], Tirtha Banerjee[3], James P.S. Neel[2]

[1]Department of Civil, Construction, and Environmental Engineering, University of Alabama, Tuscaloosa, AL, USA.

[2]USDA, Agricultural Research Service, Grazinglands Research Laboratory, El Reno, OK, USA.

[3]Department of Civil and Environmental Engineering, University of California, Irvine, CA, 92697, USA.

Corresponding author: Mukesh Kumar., 1004D Tom Bevill Bldg., 7th Ave., University of Alabama, Tuscaloosa, AL, 35401, USA (mkumar4@ua.edu)

Content of this file

Supplementary Figures

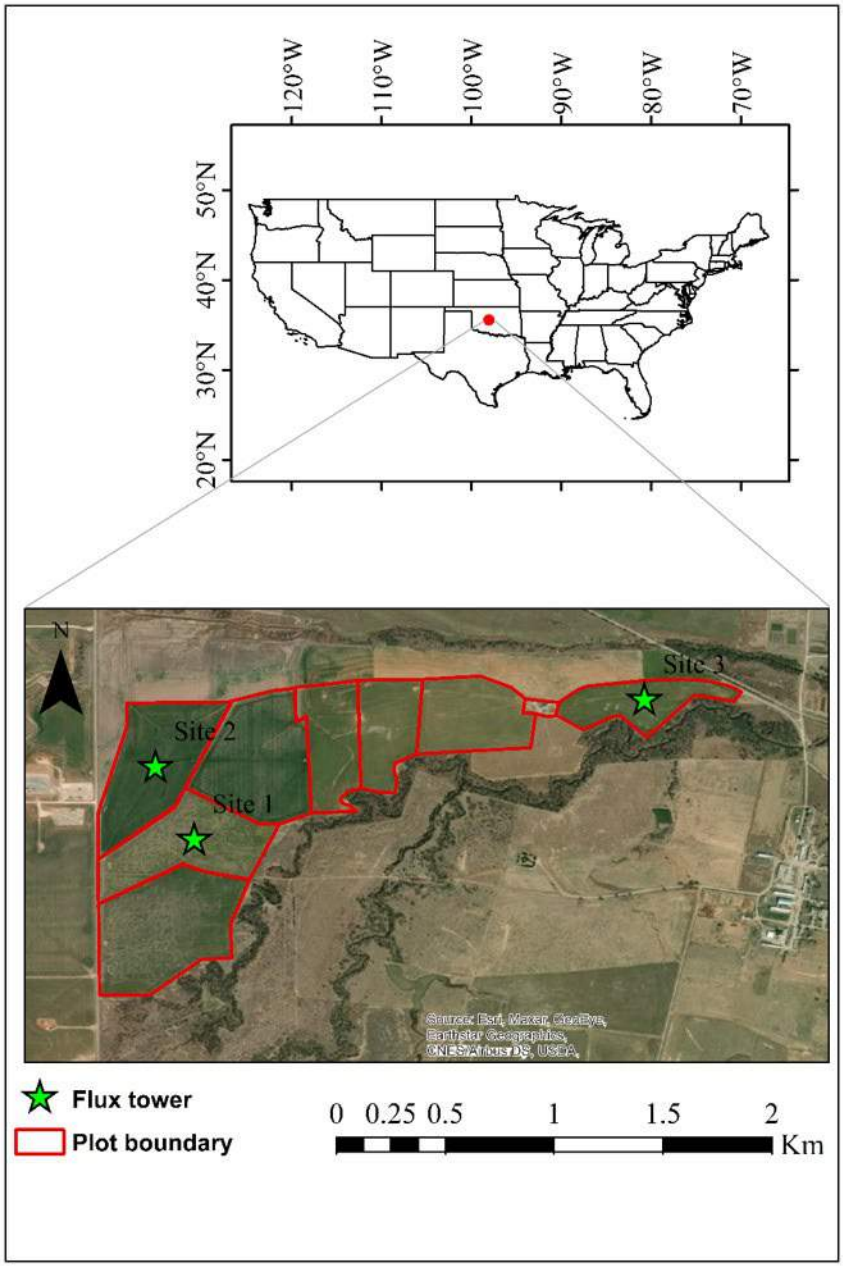

Fig. S1. Location of the three sites belonging to GRL-FLUXNET used in this study.

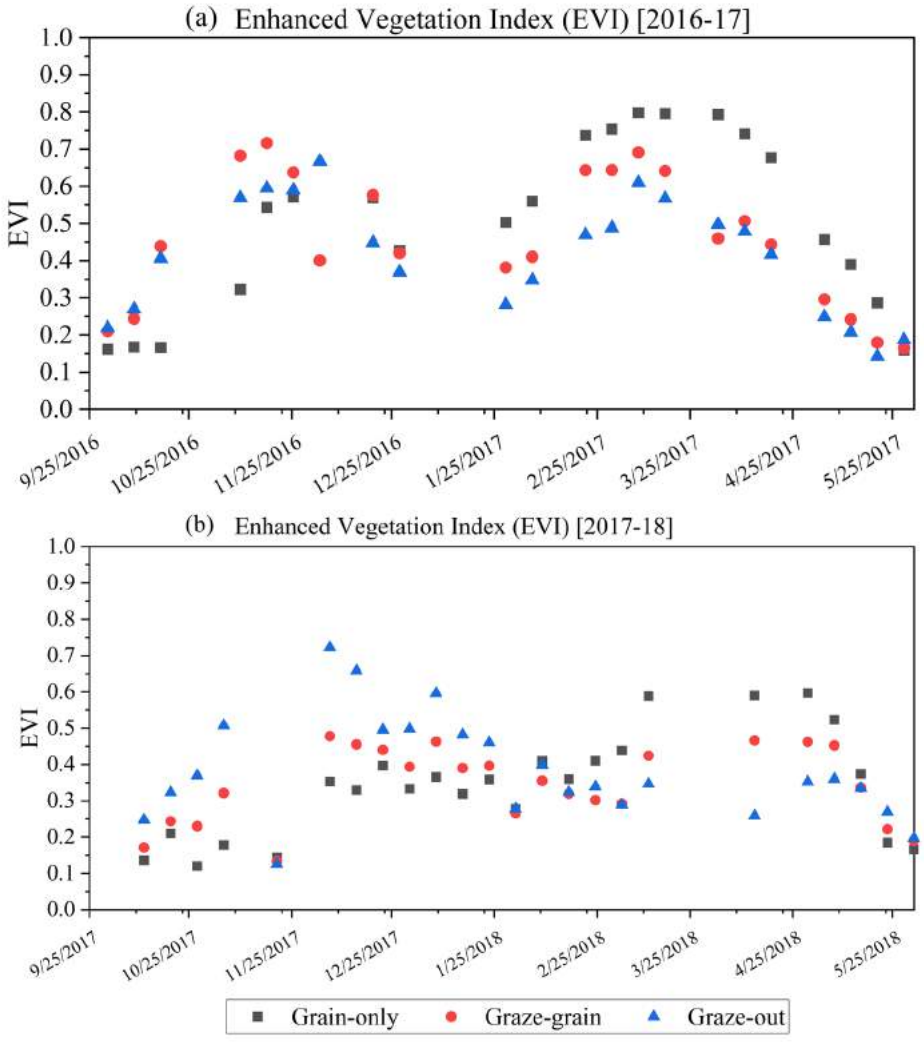

Figure S2. Landsat 7 ETM+ and Landsat 8 derived EVI for different management systems for growing seasons 2016-17 (a) and 2017-18 (b).

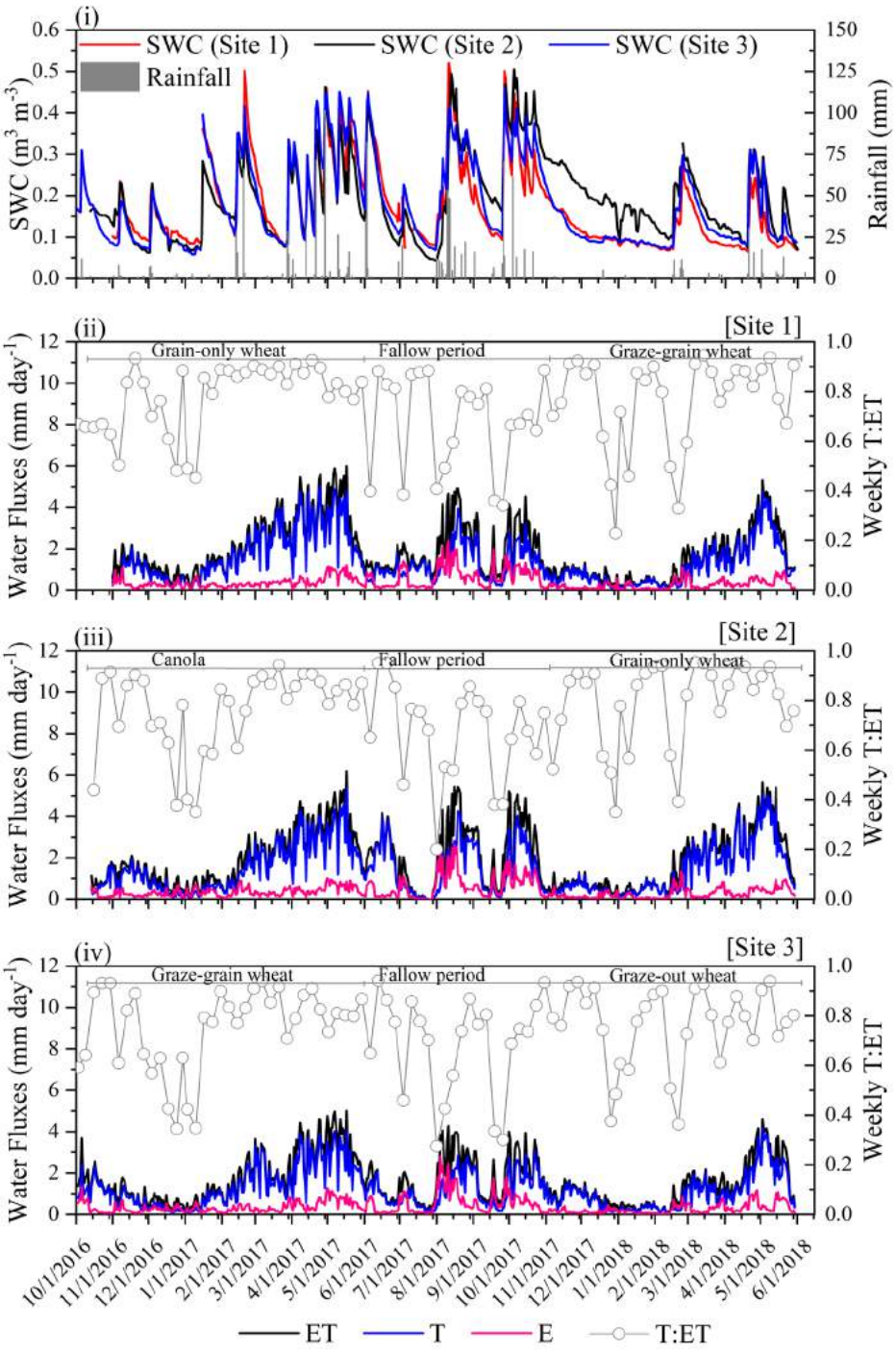

Figure S3. (i) Daily variations of rainfall and soil water content (SWC) at each site, (ii) -(iv) daily variations of total evapotranspiration (ET), transpiration (T), and direct evaporation (E) based on TEA method at three different sites. Open circles plotted on the secondary Y-axis show the ratio of weekly T and ET. Notably, all three sites underwent crop rotation. Fallow period and canola were not considered for analyses in this study.

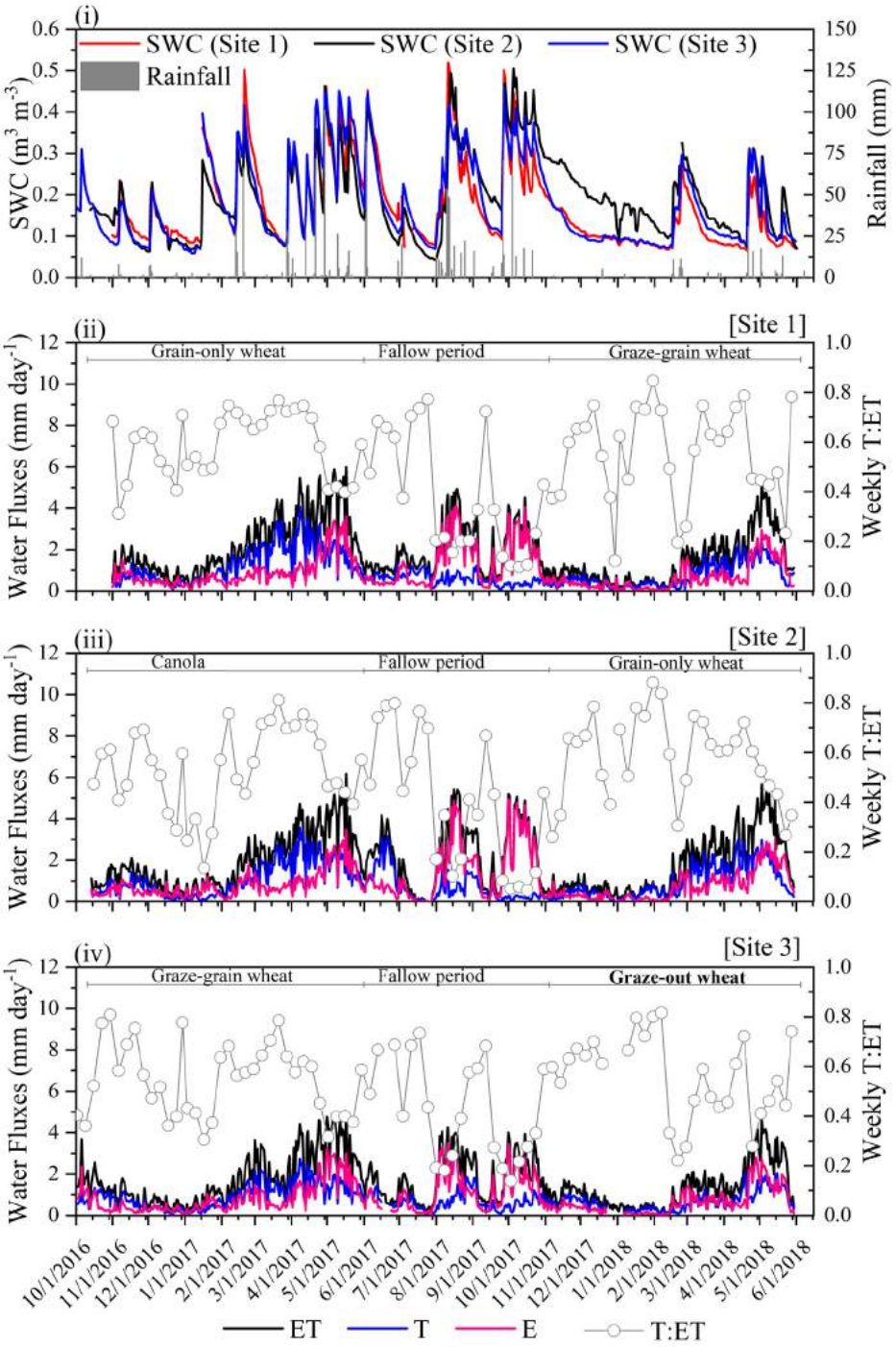

Figure S4. (i) Daily variations of rainfall and soil water content (SWC) at each site, (ii) -(iv) daily variations of total evapotranspiration (ET), transpiration (T), and direct evaporation (E) based on uWUE method at three different sites. Open circles plotted on the secondary Y-axis show the ratio of weekly T and ET. Notably, all three sites underwent crop rotation. Fallow period and canola were not considered for analyses in this study.

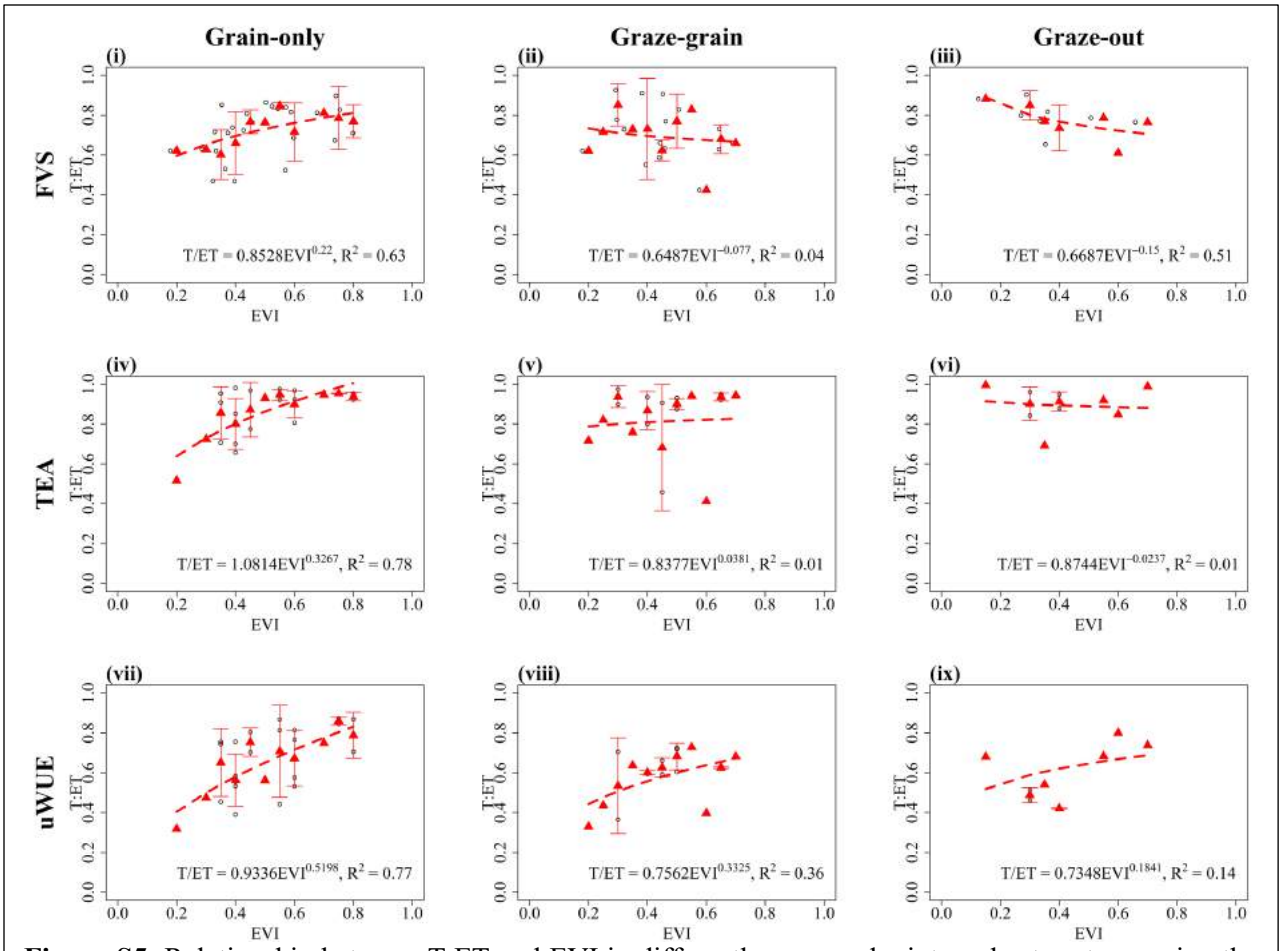

Figure S5. Relationship between T:ET and EVI in differently managed winter wheat systems using the three ET partitioning methods; FVS (i)-(iii), TEA (iv)-(vi), and uWUE (vii)-(ix), for the periods when ET partitioning estimates were available from all the three methods. Grey dots are weekly T:ET, ±3 days around the Landsat image acquisition date, during mid-day (11AM-2PM). Red triangles are averaged T:ET corresponding to 0.05-bin EVI. The vertical lines are the error bars of mean T:ET for each bin. The red dash line in each panel is the best nonlinear fit between triangles and corresponding EVI.

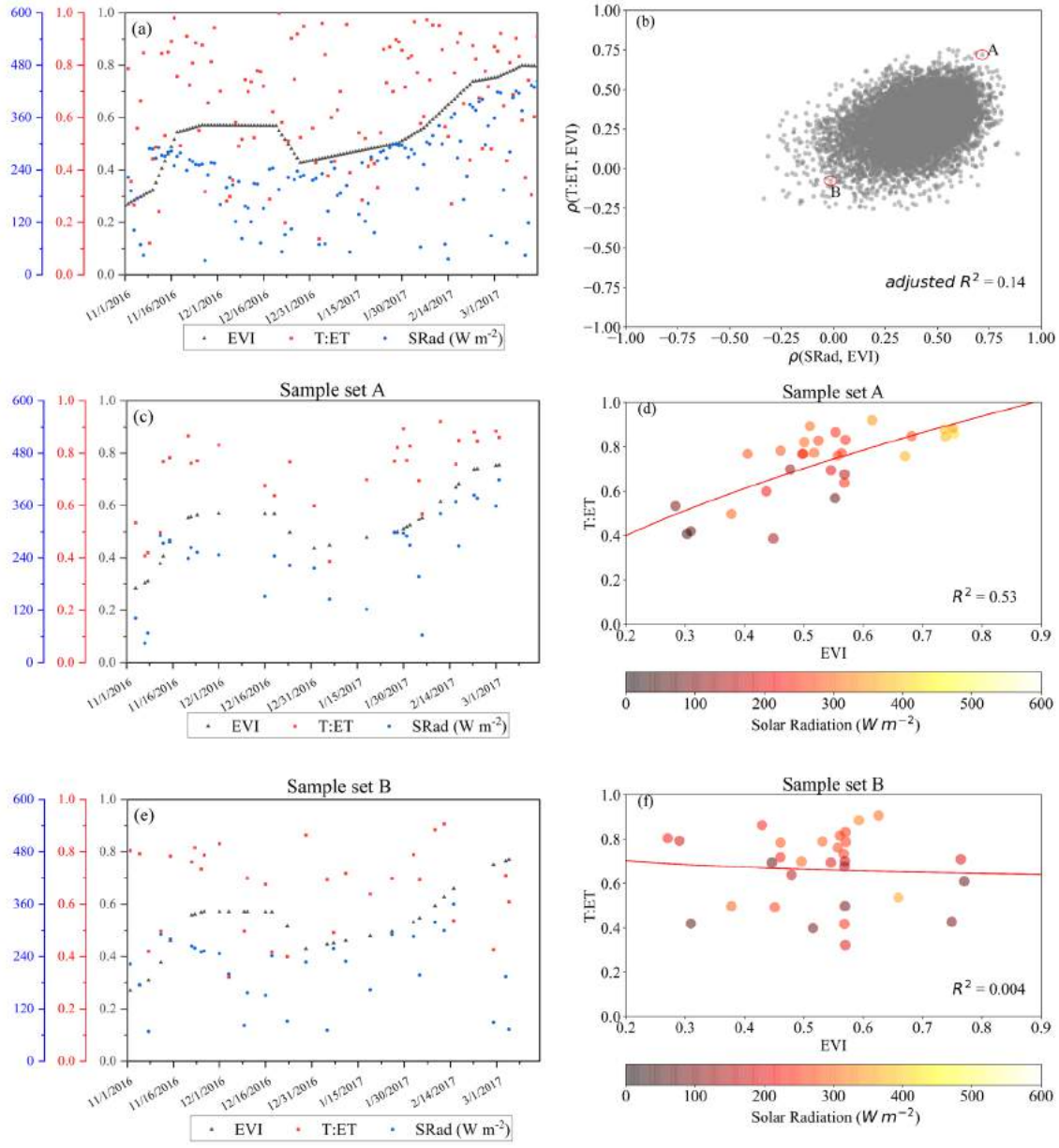

Figure S6. Temporal variations of EVI, FVS-derived T:ET, and solar radiation (SRad) for all days (a), sample set A (c), and sample set B (e). Scatter of correlation between SRad and EVI and correlation between FVS-derived T:ET and EVI for 10000 sample sets with each set having randomly selected 30 days (b). Scatter between FVS-derived T:ET and EVI for sample set A (d) and sample set B (f). Red solid lines in panels d and f represent the best-fit nonlinear lines.

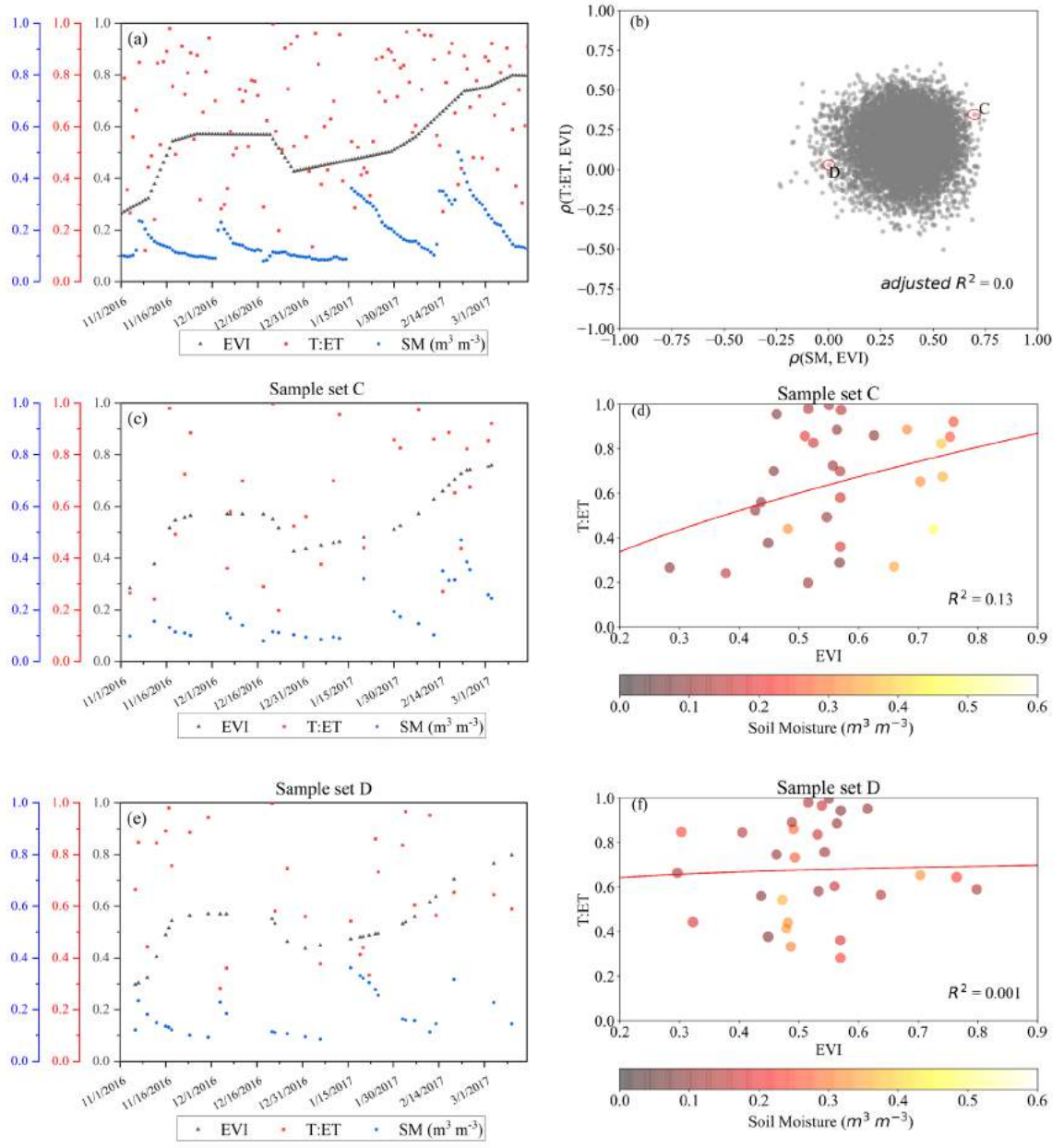

Figure S7. Temporal variations of EVI, FVS-derived T:ET, and soil moisture (SM) for all days (a), sample set C (c), and sample set D (e). Scatter of correlation between SM and EVI and correlation between FVE-derived T:ET and EVI for 10000 sample sets with each set having randomly selected 30 days (b). Scatter between FVS-derived T:ET and EVI for sample set C (d) and sample set D (f). Red solid lines in panels d and f represent the best-fit nonlinear lines.

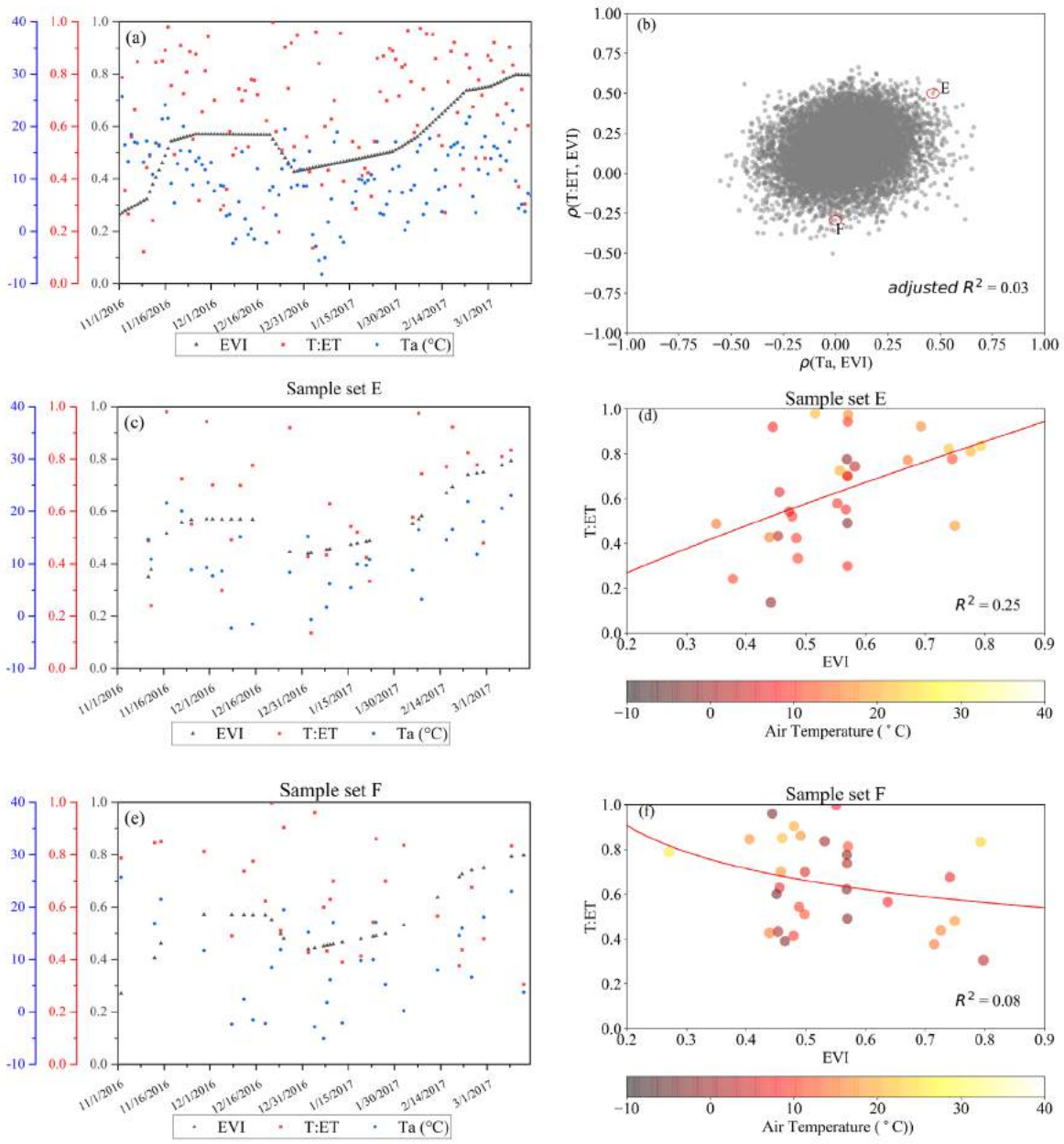

Figure S8. Temporal variations of EVI, FVS-derived T:ET, and air temperature (T_a) for all days (a), sample set E (c), and sample set F (e). Scatter of correlation between T_a and EVI and correlation between FVS-derived T:ET and EVI for 10000 sample sets with each set having randomly selected 30 days (b). Scatter between FVS-derived T:ET and EVI for sample set E (d) and sample set F (f). Red solid lines in panels d and f represent the best-fit nonlinear lines.

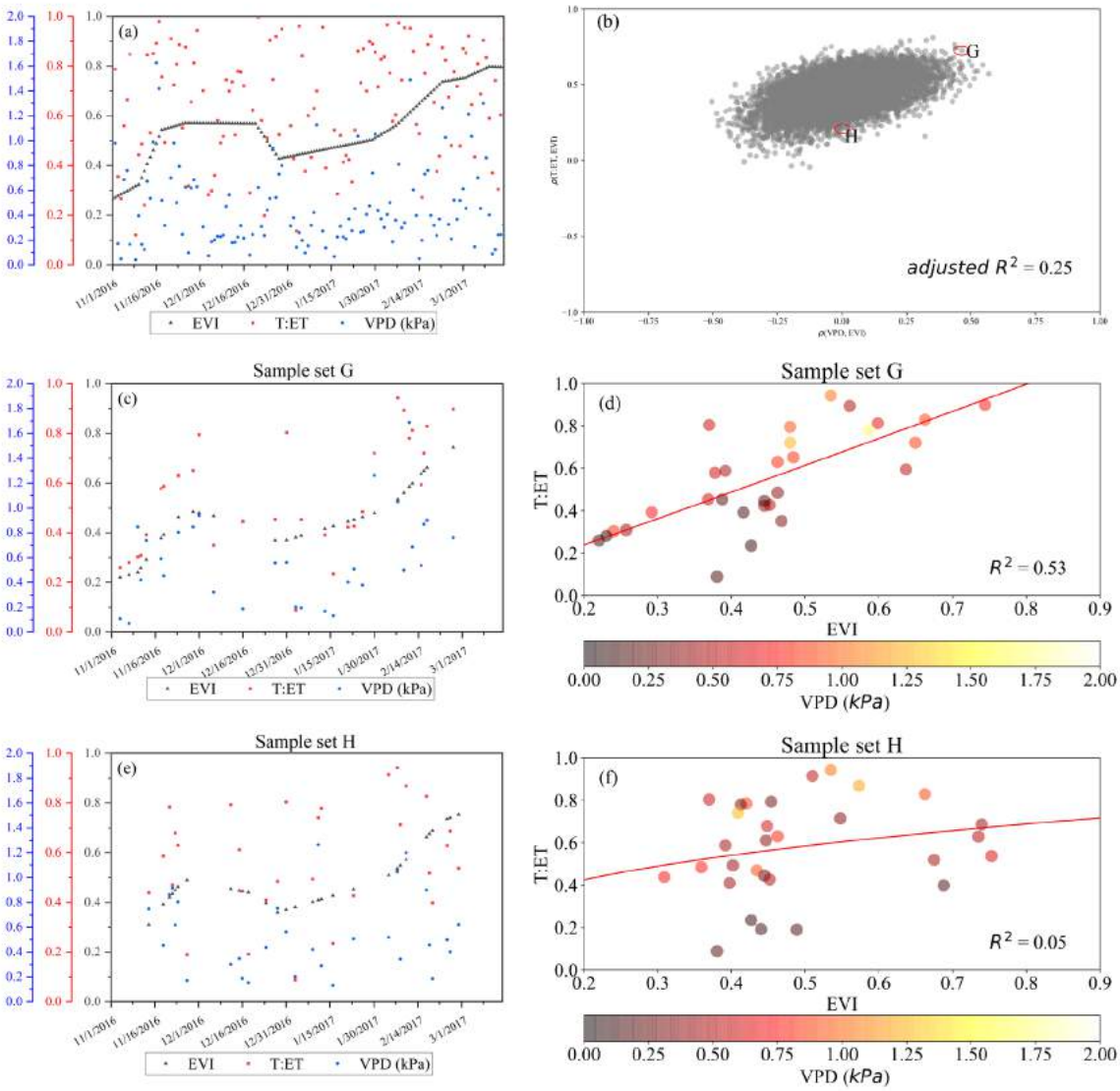

Figure S9. Temporal variations of EVI, uWUE-derived T:ET, and VPD for all days (a), sample set G (c), and sample set H (e). Scatter of correlation between VPD and EVI and correlation between uWUE-derived T:ET and EVI for 10000 sample sets with each set having randomly selected 30 days (b). Scatter between uWUE-derived T:ET and EVI for sample set G (d) and sample set H (f). Red solid lines in panels d and f represent the best-fit nonlinear lines.

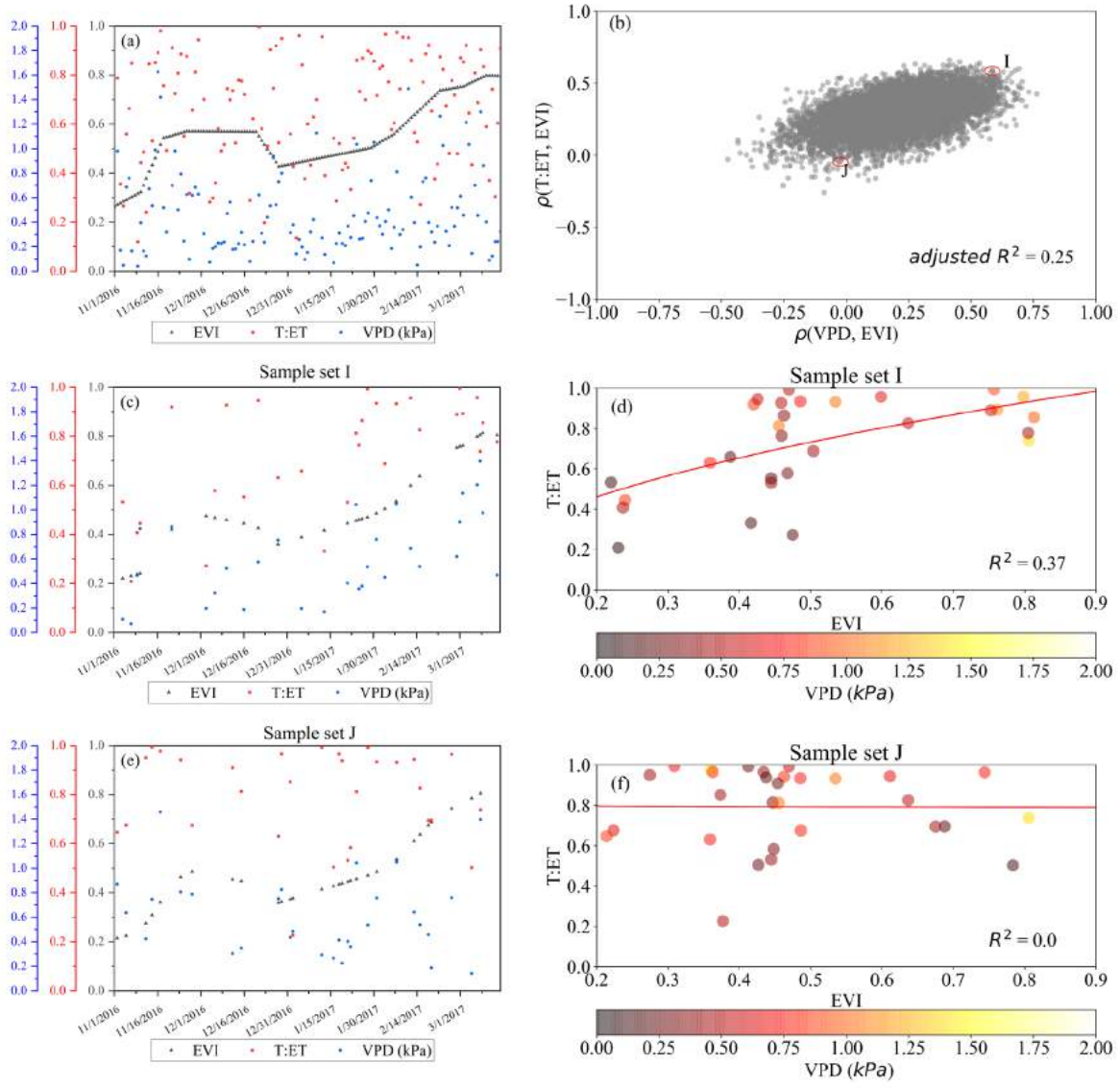

Figure S10. Temporal variations of EVI, TEA-derived T:ET, and VPD for all days (a), sample set G (c), and sample set H (e). Scatter of correlation between VPD and EVI and correlation between TEA-derived T:ET and EVI for 10000 sample sets with each set having randomly selected 30 days (b). Scatter between TEA-derived T:ET and EVI for sample set I (d) and sample set J (f). Red solid lines in panels d and f represent the best-fit nonlinear lines.

Supplementary Text

Text S1: A brief overview of the flux variance similarity-based flux partitioning

Detailed explanation on the physical and mathematical framework for the flux variance similarity (FVS)-based flux partitioning can be found elsewhere (Palatella *et al.* 2014; Scanlon and Kustas 2010; Scanlon and Sahu 2008; Scanlon *et al.* 2019; Skaggs *et al.* 2018). Here, we provide a brief overview of the FVS-based flux partitioning method.

Total carbon fluxes (F_c) measured by eddy covariance can be partition into photosynthesis (F_p) and respiration (F_r), i.e.,

$$F_c = \overline{w'c'} = F_p + F_r \quad (1a)$$

where w' is the fluctuations from the mean in vertical wind velocity (w) (i.e., $w' = w - \bar{w}$) and c' is the fluctuations from the mean in carbon concentration (c) (i.e., $c' = c - \bar{c}$). Similarly, total water fluxes (F_q) measured by eddy covariance can be partition into plant transpiration (F_t) and direct evaporation (F_e), i.e.,

$$F_q = \overline{w'q'} = F_t + F_e \quad (1b)$$

where q' is fluctuations from the mean in water vapor concentration (q) (i.e., $q' = q - \bar{q}$). FVS-based flux partitioning seeks to quantify the primary components of total carbon fluxes and total water fluxes i.e., $F_p, F_r, F_t, and\ F_e$, given the high-frequency eddy covariance measurements (e.g., 10-60 Hz) of $c, q, and\ w$.

c and q can be further decomposed as below (Scanlon and Kustas 2010; Scanlon and Sahu 2008):

$$c' = c'_p + c'_r \quad (2a)$$

$$q' = q'_t + q'_e \quad (2b)$$

where c'_p and c'_r represent fluctuations in photosynthesis and respiration, and q'_t and q'_e represent fluctuations in transpiration and direct evaporation. In terms of fluxes, equations 1a and 1b can be written as:

$$\overline{w'c'} = \overline{w'c'_p} + \overline{w'c'_r} \quad (3a)$$

$$\overline{w'q'} = \overline{w'q'_t} + \overline{w'q'_e} \quad (3b)$$

Furthermore, the stomatal fluxes (i.e., transpiration and photosynthesis) can be linked by the Water Use Efficiency (WUE) of plants at the leaf scale, which defines the coupling of photosynthesis and transpiration at the leaf scale as:

$$c'_p = WUE \times q'_t \quad (4a)$$

where their standard deviations are related as:

$$\sigma_{c_p} = -WUE \times \sigma_{q_t} \quad (4b)$$

or

$$\sigma^2_{c_p} = WUE^2 \times \sigma^2_{q_t} \quad (4c)$$

An implication of the Monin-Obukhov Similarity Theory (MOST) (Monin and Obukhov 1954) is that scalar time series measured at the same position should exhibit perfect correlation (Hill 1989), a key behind the FVS-based flux partitioning. Applying this concept between the stomatal-derived variables (i.e., $c'_p\ and\ q'_t$) and between nonstomatal variables (i.e., $c'_r\ and\ q'_e$) implies the following:

$$\rho_{c_p,q_t} = -1 \quad (5a)$$

$$\rho_{c_r,q_e} = +1 \quad (5b)$$

$$\rho_{c_p,c_r} = -\rho_{q_t,q_e} \quad (5c)$$

One more assumption involved in this theory is that transfer efficiencies of the stomatal-derived scalars (i.e., $\rho_{w,c_p}\ and\ \rho_{w,q_t}$) are greater than that of nonstomatal-derived scalars (i.e., $\rho_{w,c_r}\ and\ \rho_{w,q_e}$), because of the sources of latter being primarily situated in subcanopy air space. Based on Katul and Parlange (1995) and Bink and Meesters (1997), the following approximations are made:

$$\rho_{c_p,c_r} \approx \frac{\rho_{w,c_r}}{\rho_{w,c_p}} \quad (6a)$$

$$\rho_{q_t,q_e} \approx \frac{\rho_{w,q_e}}{\rho_{w,q_t}} \quad (6b)$$

$$\rho_{c_p,c_r} = -\rho_{q_t,q_e} \quad (6c)$$

Furthermore, variance budgets for the carbon and water vapor concentrations are written as:

$$\sigma_c^2 = \sigma_{c_p}^2 + \sigma_{c_r}^2 + 2\rho_{c_p,c_r}\sigma_{c_p}\sigma_{c_r} \quad (7a)$$

$$\sigma_q^2 = \sigma_{q_t}^2 + \sigma_{q_e}^2 + 2\rho_{q_t,q_e}\sigma_{q_t}\sigma_{q_e} \quad (7b)$$

Now, the above equations can be re-arranged to solve for the unknowns. Combining all the above equations, one can end up with a non-linear equation (see equation 15 of Scanlon and Sahu (2008)) which can be solved numerically. There have been numerous subsequent improvements in the mathematical approaches to solve equation 15 of Scanlon and Sahu (2008) (see (Palatella *et al.* 2014; Scanlon *et al.* 2019; Skaggs *et al.* 2018) for more details). One of the most important variables in the equation 15 of Scanlon and Sahu (2008) is the leaf-scale WUE which can either be measured or estimated empirically (e.g., based on the gradient approach (Campbell and Norman 2012)). Overall, the FVS-based flux partitioning approach is conceptually simple and has a strong physical and mathematical foundation. The only requirement of this approach is the high-frequency eddy covariance measurements.

Text S2: Calculation of Mean Absolute Percentage Error (MAPE)

MAPE was calculated as:

$$MAPE = \frac{100\%}{n}\sum_{i=1}^{i=n}\left|\frac{O_i - P_i}{O_i}\right| \quad (8)$$

where O_i is the ith observed T:ET value, and P_i is the ith predicted T:ET value. O_i are obtained using either of the three ET partitioning methods, i.e., FVS, TEA, and uWUE, on eddy covariance data. P_i are obtained either using the derived T:ET-EVI relations (these relations are shown in Figures 3a,d, and g) or using the global crop T:ET-LAI relation presented in Wei *et al.* (2017). It is to be noted here that the T:ET-EVI relations were derived in an undisturbed system (i.e., grain-only wheat) using weekly T:ET values for all the three ET partitioning methods.

Text S3: Factors controlling the variation of T:ET

At the ecosystem scale, the transpiration rate (T) is controlled by the stomatal conductance (g_c), atmospheric water demand (i.e., Vapor Pressure Deficit; VPD), and the plant's biophysical state (e.g., LAI). Mathematically, we can write:

$$T \propto g_c \times VPD \times LAI \quad (9)$$

g_c is further controlled by various hydro-meteorological variables, including VPD, root-zone soil moisture (θ), solar radiation (SRad), and air temperature (Daly *et al.* 2004; Jarvis 1976). i.e., $= f(VPD, \theta, SRad,)$. Notably, while g_c and T decrease with VPD (Figures S11c-d) if all other conditions remain similar, over the season T:ET shows an increasing trend with VPD (Figure S11b). It is to be noted that the increasing trend is largely controlled by the LAI, however intra-seasonal variations in VPD and radiation may mediate it.

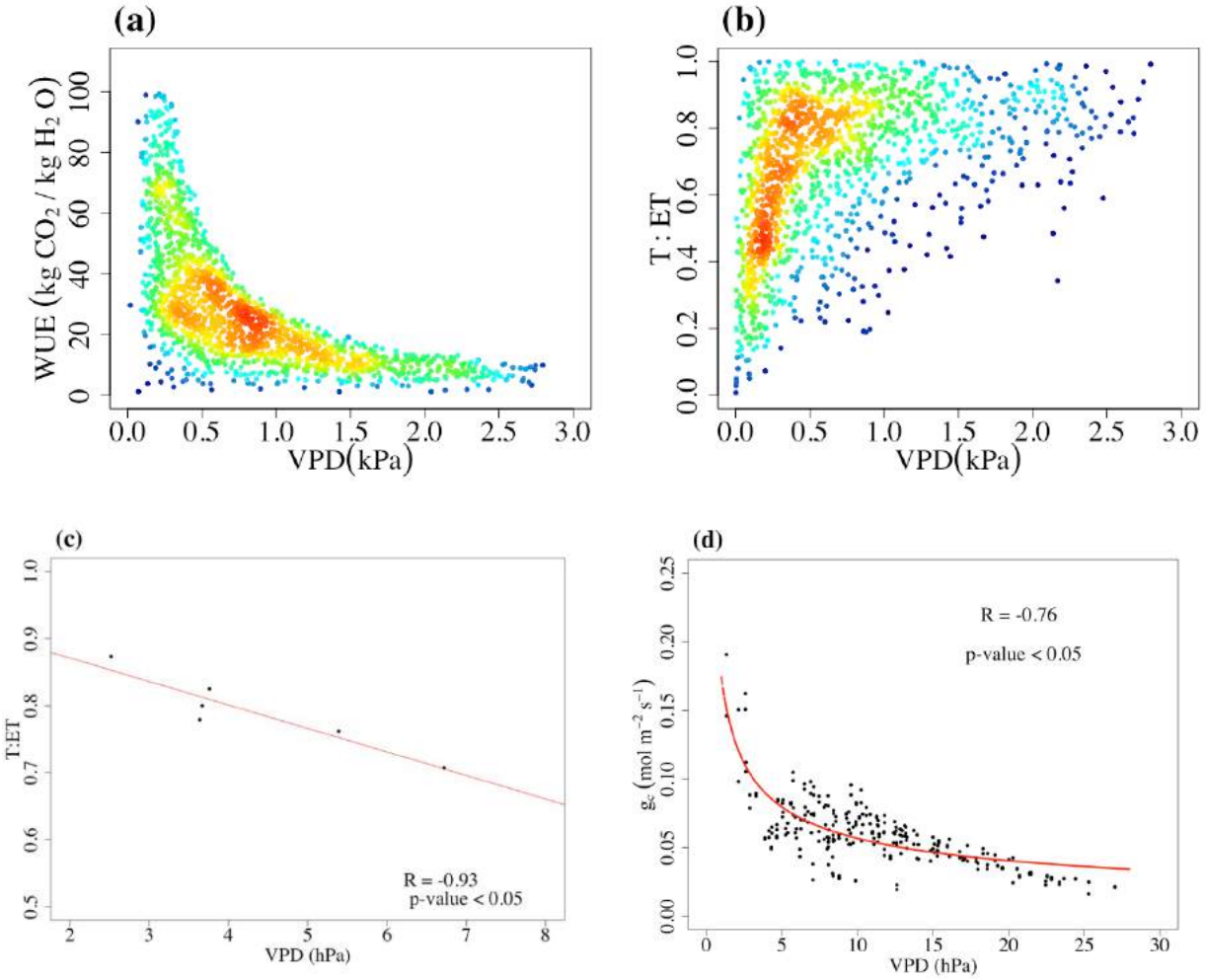

Figure S11: VPD's influence on water use efficiency (a), T:ET (b), and stomatal conductance (d) during the growing season. Control of VPD on T:ET for selected time periods (mid-days (1 PM) of Dec 01, 2016 – Dec 08, 2016) with similar conditions of solar radiation, vegetation growth, and soil moisture. The colors of the data points in panels a and b represent the relative point density with warmer colors indicating higher density.

Text S4: T:ET variation using the two-source evapotranspiration (ET) model

ET is the sum of soil evaporation (E_s) and plant transpiration (T_c). It can be formulated using a two-source ET model based on Shuttleworth and Wallace (1985) as:

$$\mathrm{ET} = \mathrm{E_s} + \mathrm{T_c} = f_s \cdot PM_s + f_c \cdot PM_c \qquad (10a)$$

$$PM_s = \frac{s \cdot A + (\rho_a \cdot C_p \cdot VPD - s \cdot r_{as}(A - A_s))/(r_{aa} + r_{as})}{s + \gamma(1 + r_{ss}/(r_{aa} + r_{as}))} \qquad (10b)$$

$$PM_c = \frac{s \cdot A + (\rho_a \cdot C_p \cdot VPD - s \cdot r_{ac} A_s)/(r_{aa} + r_{ac})}{s + \gamma(1 + r_{sc}/(r_{aa} + r_{ac}))} \quad (10c)$$

$$f_c = \frac{1}{1 + R_c \cdot R_a/(R_s(R_c + R_a))} \quad (10d)$$

$$f_s = \frac{1}{1 + R_s \cdot R_a/(R_c(R_s + R_a))} \quad (10e)$$

$$R_c = (s + \gamma) r_{ac} + \gamma \cdot r_{sc} \quad (10f)$$

$$R_s = (s + \gamma) r_{as} + \gamma \cdot r_{ss} \quad (10g)$$

$$R_a = (s + \gamma) r_{aa} \quad (10h)$$

In the above equations, subscripts s and c represent soil and canopy components, respectively. f is a weighting factor, PM is a term similar to those in the Penman-Monteith model (Monteith 1965). s is the slope of the saturation vapor pressure curve ($Pa\ K^{-1}$), A is the total available energy for sensible and latent heat flux (i.e., $A = R_n - G$; where R_n is net radiation and G is the ground heat flux) ($W\ m^{-2}$), A_s is the part of A available for soil ($W\ m^{-2}$), ρ_a is the density of the air ($kg\ m^{-3}$), C_p is the specific heat of dry air at constant pressure ($J\ kg^{-1}\ K^{-1}$), γ is the psychrometric constant ($Pa\ K^{-1}$), VPD is the vapor pressure deficit (Pa), r_{as} is the resistance to vapor transfer between the soil surface and the canopy layer ($s\ m^{-1}$), r_{aa} is the aerodynamic resistance between the canopy source and a reference height ($s\ m^{-1}$), r_{ac} is the canopy boundary layer resistance ($s\ m^{-1}$), r_{ss} is the soil surface resistance for vapor transfer ($s\ m^{-1}$), and r_{sc} is the stomatal resistance ($s\ m^{-1}$).

Additionally,

$$A = R_n - G \quad (10i)$$

$$A_s = R_{ns} - G \quad (10j)$$

$$R_{ns} = R_n \exp(-k_r \cdot LAI) \quad (10k)$$

where k_r is the canopy extinction coefficient of net radiation, and LAI is the leaf area index. Readers are encouraged to consult Shuttleworth and Wallace (1985) for an in-depth understanding of the aforementioned equations.

The calculation procedure of the different resistance terms in the above equations is well documented elsewhere. For example, to obtain aerodynamic resistances (i.e., $r_{aa}, r_{as}, and\ r_{ac}$), one can refer to Shuttleworth and Gurney (1990) and Brutsaert (2013) where these terms are being defined as the functions of canopy height, leaf structure, wind speed, friction velocity, LAI, etc. Similarly, the calculation of r_{ss} is presented in Sellers *et al.* (1992) where r_{ss} is defined as the function of soil wetness of the top soil layer. Calculation of r_{sc} can be referred in Ronda *et al.* (2001). Herein, r_{sc} (note: r_{sc} = 1/g_c) is described by a photosynthesis-stomatal conductance model, with it being dependent on a range of variables including VPD, soil moisture, radiation, and air temperature.

Based on the above equations, the ratio T/ET can be obtained as:

$$\frac{T}{ET} = \frac{f_c \cdot PM_c}{f_s \cdot PM_s + f_c \cdot PM_c} \quad (10l)$$

To understand the role of grazing on T:ET-EVI relation, we hypothesized (in Section 3.3) that the increase in T:ET with EVI (or LAI, Note: LAI and EVI are highly correlated at site scale (see Figure S12)) in undisturbed systems is strongly influenced by the covariation of VPD and EVI.

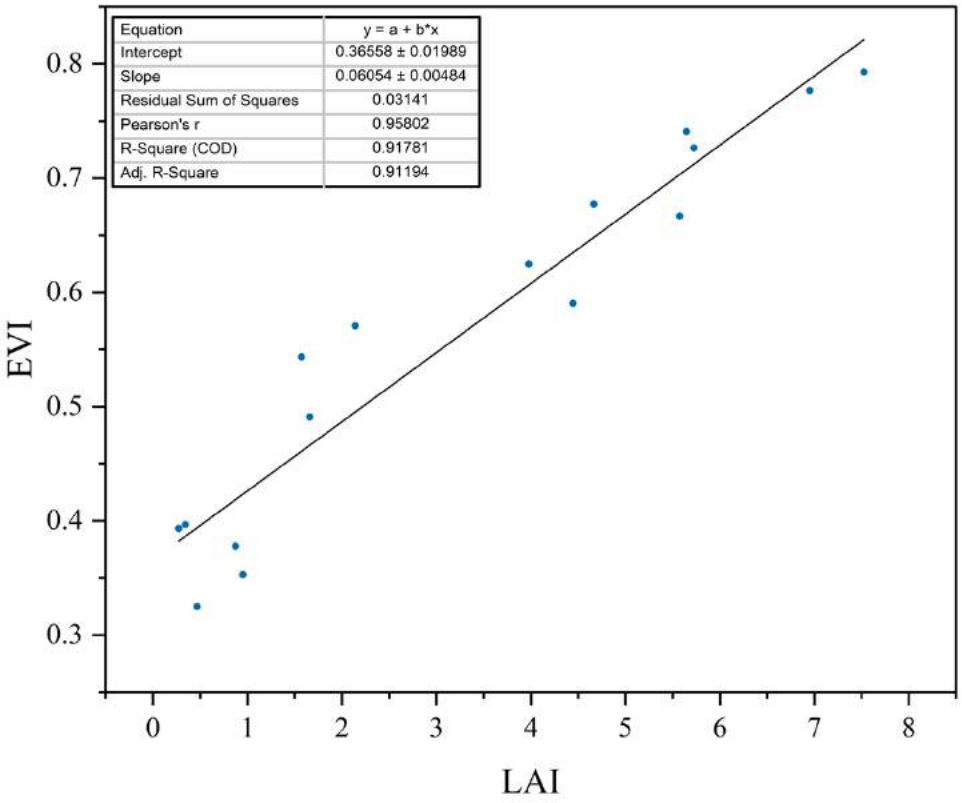

Figure S12: Comparison of field observed LAI and Landsat-derived field EVI.

However, grazing (or any other disturbances for that matter) disturbs the covariation of EVI with VPD, thus also disturbing the covariation of T:ET with EVI. Validation results concerning this hypothesis is shown in Figure 5 of the main document and Figures S9-10. We further elucidate the expressed variations using control simulations based on the two-source ET model presented above. Figure S13 plots the results from this model at daily temporal resolution for two cases; Case 1: we select 50 days during 2016-17 at site 1 such that VPD and LAI are strongly correlated for these days, Case 2: we select 50 days during 2016-17 at site 1 such that VPD and LAI are poorly correlated. Other dependent variables needed for evaluation of T:ET estimate using equation 10l are obtained based on the feeder equations 10a-k and details presented above. Even based on this two-source ET model, it is clearly evident from Figure S13 that T:ET-LAI relation is strong when VPD and LAI are positively correlated and T:ET-LAI relation is weak when VPD and LAI are poorly correlated.

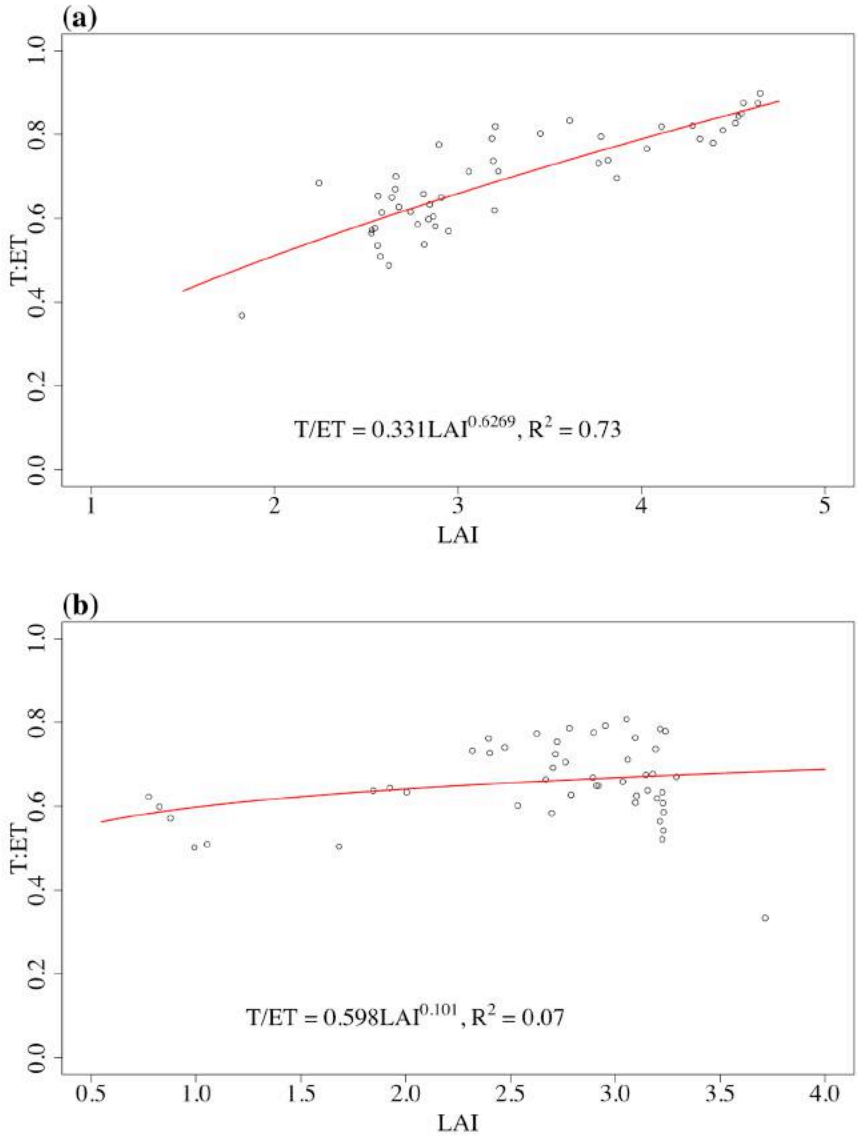

Figure S13: Variation of T:ET (simulated by Shutteleworth-Wallace two-source ET model) with LAI; (a) for the days (total 50 days) when LAI and VPD are strongly (positively) correlated, and (b) for the days (total 50 days) when LAI and VPD are poorly correlated.

Next, we explore the variations in T:ET under a range of meteorological and biomass conditions (Figures S14-S17) using the two-source ET model. Herein, we vary one dependent variable at a time. These figures primarily highlight two points: (a) LAI, VPD, solar radiation, and soil moisture all impact T:ET; (b) LAI impacts T:ET most significantly for the ranges of variables existent at the site. And so, the strength of T:ET-LAI or T:ET-EVI relation can be degraded when the seasonal covariation of EVI and hydrometeorological variables is altered.

Sensitivity to LAI:

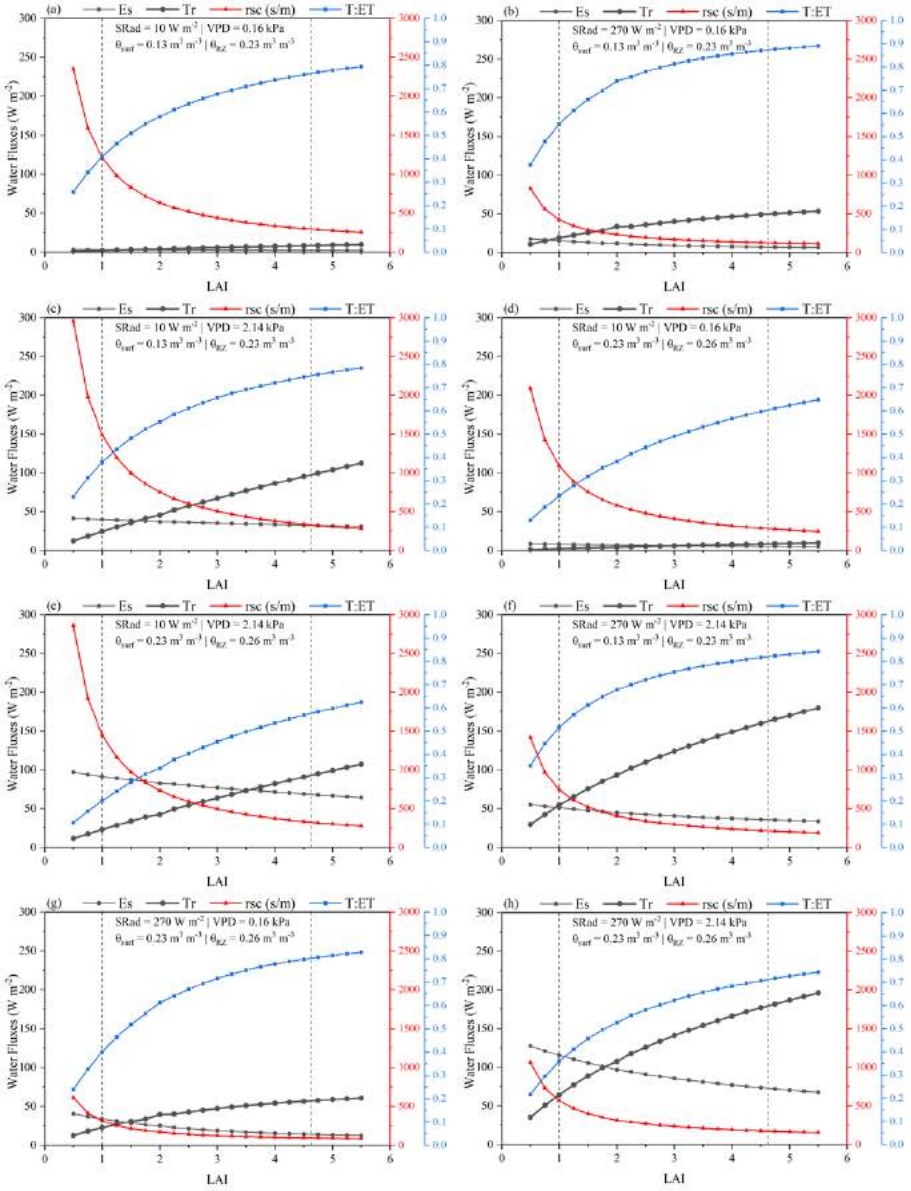

Figure S14: Variation of soil evaporation (E_s), transpiration (Tr), stomatal resistance (rsc), and T:ET (based on Shuttleworth-Wallace two-source ET model) with LAI. Panels a-h show the variation under different conditions of SRad, VPD, surface soil moisture (θ_{surf}) and root-zone soil moisture (θ_{RZ}). Two vertical dashed lines added in each panel represent the 15th and 85th percentile values of LAI observed at site 1.

Sensitivity to VPD:

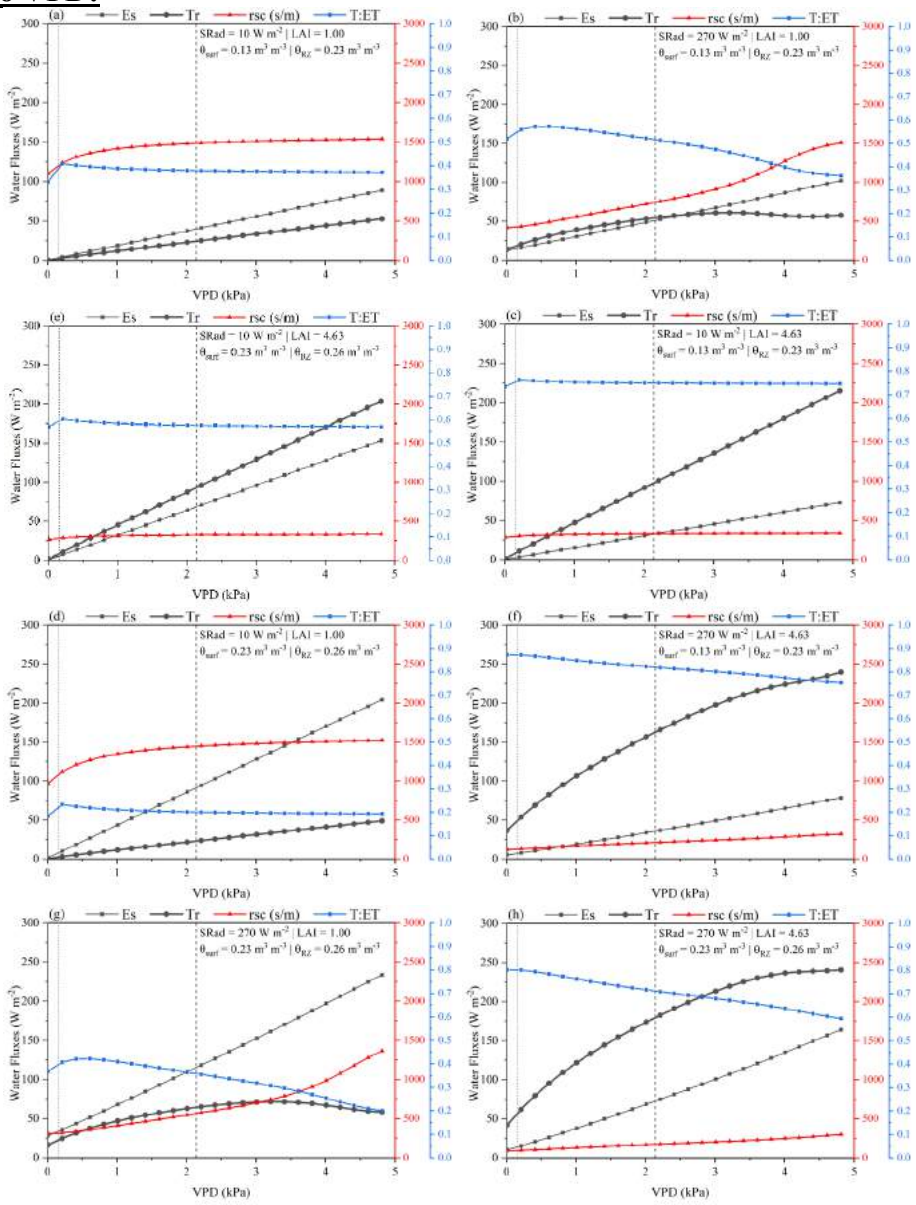

Figure S15: Variation of soil evaporation (E_s), transpiration (Tr), stomatal resistance (rsc), and T:ET (based on Shutteleworth-Wallace two-source ET model) with VPD. Panels a-h show the variation under different conditions of SRad, LAI, surface soil moisture (θ_{surf}) and root-zone soil moisture (θ_{RZ}). Two vertical dashed lines added in each panel represent the 15th and 85th percentile values VPD observed at site 1.

Sensitivity to Solar Radiation (SRad) or Net Radiation:

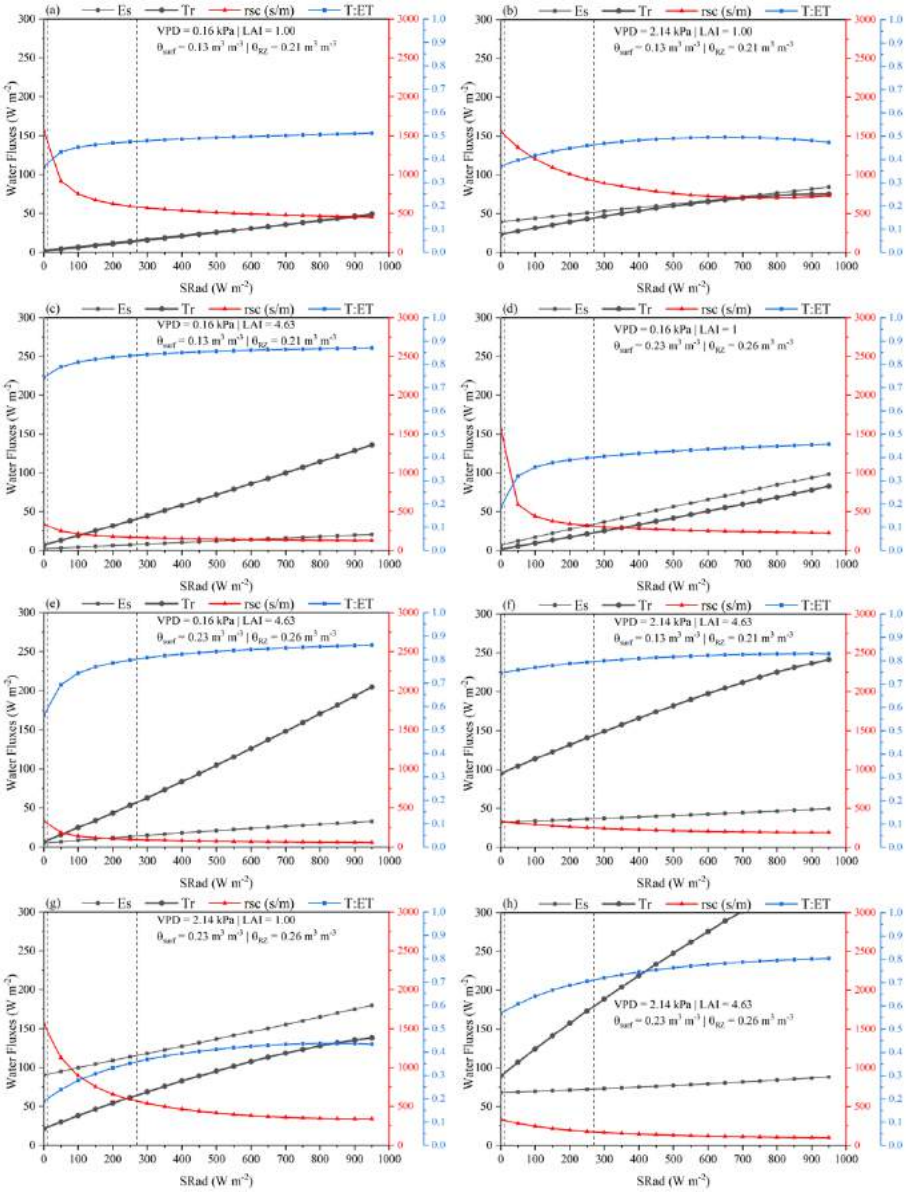

Figure S16: Variation of soil evaporation (E_s), transpiration (Tr), stomatal resistance (rsc), and T:ET (based on Shutteleworth-Wallace two-source ET model) with solar radiation (Srad). Panels a-h show the variation under different conditions of vapor pressure deficit (VPD), LAI, surface soil moisture (θ_{surf}) and root-zone soil moisture (θ_{RZ}). Two vertical dashed lines added in each panel represent the 15th and 85th percentile values of solar radiation observed at site 1.

Sensitivity to soil moisture:

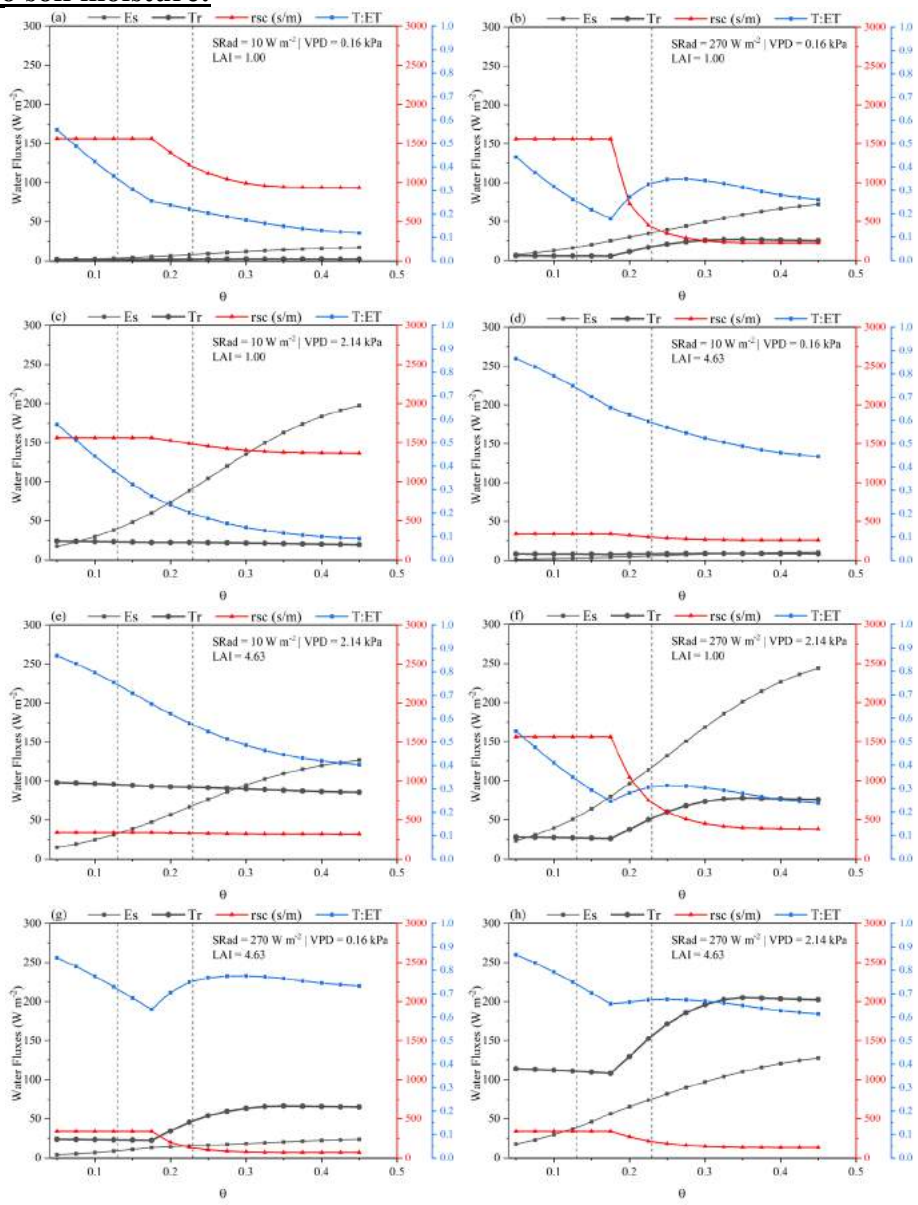

Figure S17: Variation of soil evaporation (E_s), transpiration (Tr), stomatal resistance (rsc), and T:ET (based on Shutteleworth-Wallace two-source ET model) with soil moisture (θ). Panels a-h show the variation under different conditions of SRad, VPD, and LAI. Two vertical dashed lines added in each panel represent the 15th and 85th percentile values of θ observed at site 1.

References

Bink, N. and Meesters, A. 1997. Comment on 'Estimation of surface heat and momentum fluxes using the flux-variance method above uniform and non-uniform terrain'by Katul et al.(1995). Boundary-layer meteorology 84(3), 497-502.

Brutsaert, W. (2013) Evaporation into the atmosphere: theory, history and applications, Springer Science & Business Media.

Campbell, G.S. and Norman, J. (2012) An introduction to environmental biophysics, Springer Science & Business Media.

Daly, E., Porporato, A. and Rodriguez-Iturbe, I. 2004. Coupled dynamics of photosynthesis, transpiration, and soil water balance. Part I: Upscaling from hourly to daily level. Journal of Hydrometeorology 5(3), 546-558.

Hill, R.J. 1989. Implications of Monin–Obukhov similarity theory for scalar quantities. Journal of Atmospheric Sciences 46(14), 2236-2244.

Jarvis, P. 1976. The interpretation of the variations in leaf water potential and stomatal conductance found in canopies in the field. Philosophical Transactions of the Royal Society of London. B, Biological Sciences 273(927), 593-610.

Katul, G.G. and Parlange, M.B. 1995. Analysis of land surface heat fluxes using the orthonormal wavelet approach. Water Resources Research 31(11), 2743-2749.

Monin, A.S. and Obukhov, A.M. 1954. Basic laws of turbulent mixing in the surface layer of the atmosphere. Contrib. Geophys. Inst. Acad. Sci. USSR 151(163), e187.

Monteith, J.L. 1965 Evaporation and environment, pp. 205-234, Cambridge University Press (CUP) Cambridge.

Palatella, L., Rana, G. and Vitale, D. 2014. Towards a flux-partitioning procedure based on the direct use of high-frequency eddy-covariance data. Boundary-layer meteorology 153(2), 327-337.

Ronda, R., De Bruin, H. and Holtslag, A. 2001. Representation of the canopy conductance in modeling the surface energy budget for low vegetation. Journal of Applied Meteorology 40(8), 1431-1444.

Scanlon, T.M. and Kustas, W.P. 2010. Partitioning carbon dioxide and water vapor fluxes using correlation analysis. Agricultural and Forest Meteorology 150(1), 89-99.

Scanlon, T.M. and Sahu, P. 2008. On the correlation structure of water vapor and carbon dioxide in the atmospheric surface layer: A basis for flux partitioning. Water Resources Research 44(10).

Scanlon, T.M., Schmidt, D.F. and Skaggs, T.H. 2019. Correlation-based flux partitioning of water vapor and carbon dioxide fluxes: Method simplification and estimation of canopy water use efficiency. Agricultural and Forest Meteorology 279, 107732.

Sellers, P.J., Heiser, M.D. and Hall, F.G. 1992. Relations between surface conductance and spectral vegetation indices at intermediate (100 m2 to 15 km2) length scales. Journal of Geophysical Research: Atmospheres 97(D17), 19033-19059.

Shuttleworth, W.J. and Gurney, R.J. 1990. The theoretical relationship between foliage temperature and canopy resistance in sparse crops. Quarterly Journal of the Royal Meteorological Society 116(492), 497-519.

Shuttleworth, W.J. and Wallace, J. 1985. Evaporation from sparse crops-an energy combination theory. Quarterly Journal of the Royal Meteorological Society 111(469), 839-855.

Skaggs, T.H., Anderson, R.G., Alfieri, J., Scanlon, T. and Kustas, W. 2018. Fluxpart: Open source software for partitioning carbon dioxide and water vapor fluxes. Agricultural and Forest Meteorology 253, 218-224.

Wei, Z., Yoshimura, K., Wang, L., Miralles, D.G., Jasechko, S. and Lee, X. 2017. Revisiting the contribution of transpiration to global terrestrial evapotranspiration. Geophysical Research Letters 44(6), 2792-2801.